TRANSITION METAL OXIDES (TMOs) BASED SUPERCAPCITORS APPLICATIONS

TRANSITION METAL OXIDES (TMOs) BASED SUPERCAPCITORS APPLICATIONS

By: AKANSHA SEERVI, B. Tech

A Thesis Submitted to the School of Graduate Studies in Partial Fulfilment of the Requirements for the Degree of a Master of Applied Science

McMaster University

McMaster University

Hamilton, Ontario

TITLE	TRANSITION METAL OXIDES (TMOs) BASED SUPERCAPACITORS
AUTHOR	Akansha Seervi
SUPERVISORS	Dr. Seshasai Srinivasan Dr. Amin Reza Rajabzadeh
NUMBER OF PAGES	xiii, 70

Lay Abstract

Supercapacitors are energy storage devices that can replace traditional batteries in a few years. Their importance is defined by faster charging, higher capacity, and energy density. Therefore, it is crucial to create new materials that can advance the applications of supercapacitors. In this thesis, a novel sodium hexa-titanate material was synthesized and studied using electrochemical techniques to evaluate the material based on its capacitance. The combined use of characterization, electrochemical techniques, and the synthesis of sodium hexa-titanates grown on the Ti substrate has been successful.

Abstract

Energy storage devices, such as supercapacitors, have replaced fuel cells, batteries, and traditional capacitors. Herein, a novel method is introduced to build supercapacitors from sodium hexa-titanates grown directly from a titanium dioxide (TiO_2) substrate that has shown remarkable capacitance. Sodium hexa-titanates ($Na_2Ti_6O_{13}$) nanostructures exhibit a high electrochemical surface area and unique structural properties. The research implements the use of electrochemical and characterization techniques. Furthermore, sodium hexa-titanates were investigated for supercapacitance by doping oxygen vacancies and modifying them with trace amounts of ruthenium (Ru) to form nanostructured composites. A hybrid-based nanostructure combines sodium hexa-titanate with Co_3O_4 nanoparticles to successfully create electrode materials. An electrochemical reduction method was used to induce oxygen vacancies into the lattice structure of Ti/$Na_2Ti_6O_{13}$ nanocomposites and enhance electrochemical and pseudo-capacitance properties. Thus, sodium hexa-titanates have great potential to build the next generation of supercapacitors.

Acknowledgments

I want to thank my supervisors, Dr. Amin Reza Rajabzadeh and Dr. Seshasai Srinivasan, who have demonstrated all the characteristics of amazing mentors. I am grateful for Dr. Rajabzadeh's for his encouragement in all my endeavours since undergraduate. I also thank Dr. Seshasai Srinivasan ensure that my experience as a graduate student had the perfect balance between research and technicalities. Thank you also to Dr. Jesse Dondapati and Akhtar Bayat for their guidance. Their responses to all my beginner questions gave me the confidence to keep asking questions and making me a confident researcher. I also want to thank the BioX Lab Group for their help throughout my years as a graduate student.

Thank you to Dr. Igor Zhitomirsky for being part of my defence committee and for his guidance during my committee meetings. His comments encouraged me to reconsider important sections of my research. I want to express my gratitude to my family for their unconditional love and for always being there for me. I would also like to thank my best friend, Anna, for being there with me and the most amazing person in my life.

Table of Contents

List of Figures

List of Tables

List of Equations

List of Abbreviations

EC	Electrochemical Capacitors
EDLC	Electric double layer capacitors
HEV	Hybrid electric vehicles
$Na_2Ti_6O_{13}$	Sodium Hexa-Titanates
TiO_2	Titanium Dioxide
RuO_2	Ruthenium oxide
Co_3O_4	Cobalt oxide
TMOs	Transition metal oxides
ECSCs	Electrochemical supercapacitors
LIBs	Lithium-ion batteries
UPD	Underpotential deposition
EASA	Electrochemical active surface area
CV	Cyclic voltammetry
GCD	Galvanostatic charge discharge
EIS	Electrochemical impedance spectroscopy
XRD	X-ray crystallography
ESEM	Environmental scanning electron microscopy
XPS	X-ray photoelectron spectroscopy

Chapter 1. Introduction

1.1. Motivation

Energy consumption have immensely contributed to extensive research and development of new alternative energy sources. Industrial and technological breakthroughs have dramatically increased global energy consumption in the past decades. Renewable energy resources like solar and wind energies can fulfill global demands sustainably. However, their real-world integration is challenged because of the current inadequate energy storage mechanisms to deal with the intermittent nature of wind and solar energy [1,2]. Among many energy storage devices, batteries and supercapacitors are the main electrochemical energy storage technologies. Electrochemical supercapacitors (ECSCs) have a similar system mechanism to conventional capacitors and uses electrode and electrolyte interfaces for energy storage [2,3]. Present-day energy storage solutions like batteries although popular, are expensive and unsustainable. Therefore, there is an urgency to close the research gap in energy storage technologies. Current research is based on carbon-based materials; however, they suffer from long cycle life. There is a need to develop new materials for testing the combination of nanotechnology and electrochemistry to enhance the efficiencies of supercapacitors.

1.2. Objectives

The main objectives of this project are to exploit the high surface area of Transition Metal Oxide (TMOs) specifically Sodium Hexa-Titanates ($Na_2Ti_6O_{13}$) nanowires known for its high pseudo capacitance. The project mainly focuses on improvement of electric double layer capacitance (EDLC) with pseudo capacitance to develop the high-performance supercapacitors. The objective is to develop the cost-effective TMO based sodium hexa titanates grow directly on Ti substrate and introduce oxygen vaccines into the lattice structure of $Na_2Ti_6O_{13}$ to increase overall supercapacitance. To create the synergistic effect of materials, sodium hexa-titanates nanowires were modified with transition metal ions such as ruthenium and nanoparticles such as cobalt oxide (Co_3O_4). This will create a competitive or enhanced material devoid of carbon materials. The objectives were pursued through several electrochemical techniques.

1.3. Thesis Outline

The thesis is arranged as follows

Chapter 2 focuses on literature review on fuels cell, batteries, capacitors and supercapacitors, mechanism of energy storage and transition metal oxides. Chapter 3 focuses on Sodium hexa-titanate nanocomposites modified with trace amounts of ruthenium displaying enhanced supercapacitance. Chapter 4 focuses on Sodium hexa-titanate and Cobalt oxides nanocomposites displaying enhanced supercapacitance. Chapter 5 summarizes the work, presenting the conclusion and potential future work.

1.4. References

[1] J. Mitali, S. Dhinakaran, and A. A. Mohamad, "Energy storage systems: a review," *Energy Storage and Saving*, vol. 1, no. 3, pp. 166–216, Sep. 2022, doi: 10.1016/j.enss.2022.07.002.

[2] J. Zhang, M. Gu, and X. Chen, "Supercapacitors for renewable energy applications: A review," *Micro and Nano Engineering*, vol. 21, p. 100229, Dec. 2023, doi: 10.1016/j.mne.2023.100229.

[3] A. C. Forse, C. Merlet, J. M. Griffin, and C. P. Grey, "New Perspectives on the Charging Mechanisms of Supercapacitors," *J. Am. Chem. Soc.*, vol. 138, no. 18, pp. 5731–5744, May 2016, doi: 10.1021/jacs.6b02115.

Chapter 2. Literature Review

2.1. Fuels cells, batteries, supercapacitors

Electrochemical storage devices and conversions include fuel cells, batteries, capacitors and supercapacitors. Fuel cells and batteries convert chemical energy into electrical energy by redox electrode reactions. Batteries can store limited energy, whereas fuel cells have a continuous fuel supply [1] [2]. Fuel cells have potential applications in transportation and electronic devices such as smartphones, tablets, etc. [3-5]. There is ongoing research and development on batteries to improve their energy cycle life, increase energy/power density, and reduce cost [5]. The most important energy storage systems are Lithium-ion batteries (LIBs) and supercapacitors. Conventional capacitors store charge at the surface of electrodes and release it when required, but they can't store large amounts of energy.

Supercapacitors, also known as electrochemical capacitors (EC), are complementary to batteries' performance and are high-power devices with limited long cycle life and energy storage capability [6][7]. They yield higher power density but have low energy density, which results in long process times, from seconds to minutes. ECs can operate at a higher rate of discharge or charge cycles over almost unlimited cycles. LIBs are best in performance with significant energy densities of about 180 watts hours per kg (Wh/kg); there have been significant efforts in developing Li-ion and other secondary batteries [8]. Though LIBs have significant usage in various applications in electric vehicles and electronics, they lack power density and short cycling stability, which can restrict their commercial use [9]. Batteries are used in applications where small current densities are

required for long periods. Some applications include cell phones, laptops, tablets or small to medium-energy applications [10].

Supercapacitors are high-performance devices that can integrate the characteristics of conventional capacitors and batteries [11] [12]. They have shown high chances of reversibility in charge-discharging cycles, extending cycle life by 500,000 cycles [13]. Classic supercapacitor applications are braking systems for hybrid electric vehicles (HEV) that occur in a few seconds [10]. The Ragone plot, which shows power density plotted against energy density, shows the performance of different ESS systems [14]. It indicates supercapacitors cover several power and energy density magnitudes. Electric double-layer capacitors (EDLC) and pseudo capacitance are two types of supercapacitors.

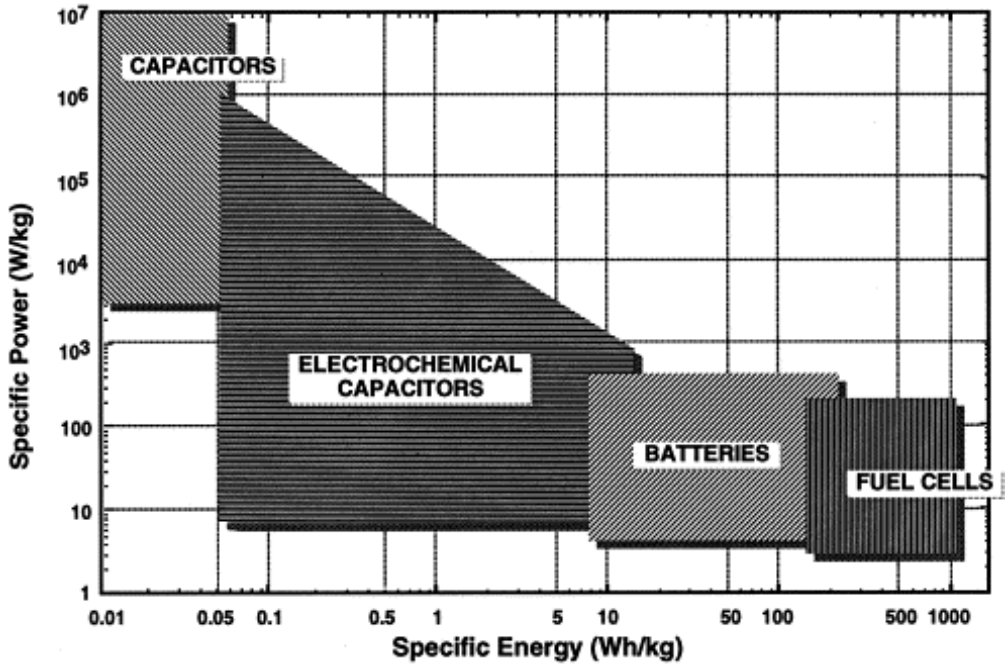

Figure 2-1: Ragone plots for energy storage system [15]

2.2. Electric double layer capacitors

Electric double-layer capacitors (EDLC) charge electrostatically and store more energy than conventional capacitors [16]. The EDLC collector is separated by a liquid electrolyte, either aqueous or organic [17] [18]. The electric double layer consists of two parallel electrodes with dielectric interlayers. The arrangement can lead charges on both sides until equilibrium [19]. EDLCs accumulate charge on high surface areas, and no faradic reactions are involved; therefore, they exhibit higher charge-discharge cycles than batteries [20].

The earliest EDLC model was developed by Helmholtz, who treated the double layers as conventional capacitors. According to Helmholtz, charged ions are arranged in an array at the surface; after several modifications by Gouy and Chapman, the diffusion layer was formed [21]. Later, Stern combined the Helmholtz, Gouy, and Chapman models, giving an internal layer (Helmholtz layer) and an external diffusion layer, as shown in *Figure 2-2* [22].

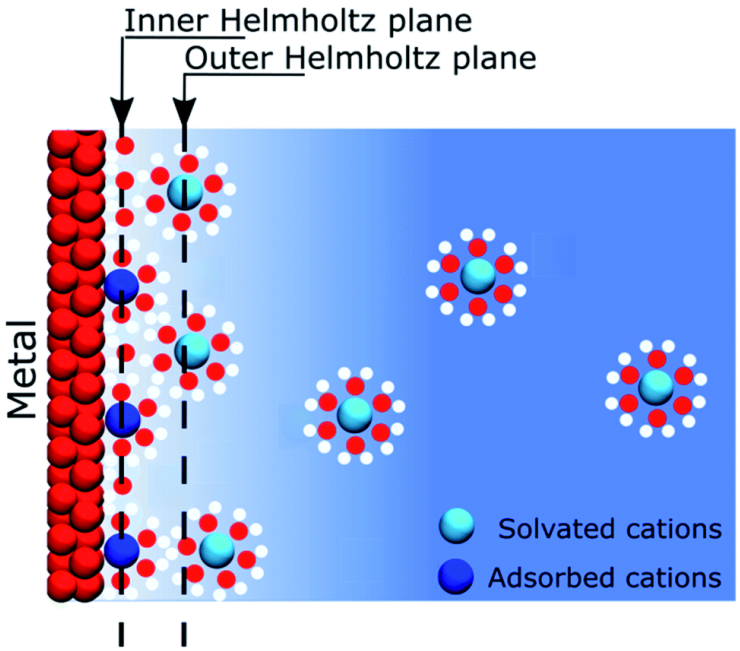

Figure 2-2: Representation of double layer mechanism of electrode interface based on Stern-Gouy-Chhapman model [23]

The first patent material for EDLC concept supercapacitors was carbon-based materials; materials can range from carbon nanotubes [24], activated carbon [25], graphite [26], graphene [27], mesoporous carbon [28], reduced graphene oxide [29]. The size of the porous electrode and electrolyte contributes to the creation of the double layer [30]. Carbon-based materials have an extensive surface area (2500 m^2/g) and electrical conductivity. They are environmentally friendly and excellent candidates for EDLC [31][32]. The ions that accumulate on the electrode surface increase due to a higher specific area of carbon. The carbon's electrode-specific capacitance is summarized in *Table 2-1*. Poor wettability in an electrolyte solution hindered the performance of carbon-based materials by reducing the area accessibility for the formation of a double layer (EDL). Ions are transported via porous carbon pores during the charge-discharge process, resulting in poor wettability and high resistance. Several chemical surface modifications have been conducted to improve the wettability of the electrode [33].

Table 2-1: Comparison between the different EDLC carbon-based materials.

Materials	Specific capacitance	Types of Electrolytes	References
Carbon aerogels	152 Fg^{-1}	Organic	[34]
Phenolic resin-based carbon	160 Fg^{-1}	Organic	[35]
PAN fibers	371 Fg^{-1}	Aqueous	[36]
Activated Carbon	78.2 Fg^{-1}	Polymer	[37]
Biomass based activated carbon	321 Fg^{-1}	Aqueous	[38]
Biocarbon	110.8 Fg^{-1}	Aqueous	[39]

2.3. Pseudo Capacitance

Pseudo-capacitance is defined for materials that exhibit electrochemical properties similar to conventional capacitors [40]. The materials that primarily exhibit redox behaviour are transition metal-oxides (TMOs) and conducting polymers. The multiple valence states in TMOs cause their pseudocapacitive behaviour [41][42]. The pseudo capacitors have different charge storage mechanisms where reactions are faradic at the origin through fast redox processes at the electrode surface [43]. It can represent a capacitor; these pseudo capacitors also reflect on quasi-rectangular cyclic voltammetry (CVs) and triangular galvanostatic charge-discharge curves (GCD) [44]. Pseudocapacitive materials have better capacitance than a double layer but poor cycle life [45]. The pseudo capacitors' charge mechanisms involve either near or surface redox or intercalation reactions [46]. There has been significant development in materials, mainly for metal oxides and conducting polymers, where they offer benefits compared to carbon materials. There have three types of mechanisms exist for pseudo capacitance: 1) Underpotential deposition, 2) Redox pseudo capacitance, 3) Intercalation pseudo capacitance.

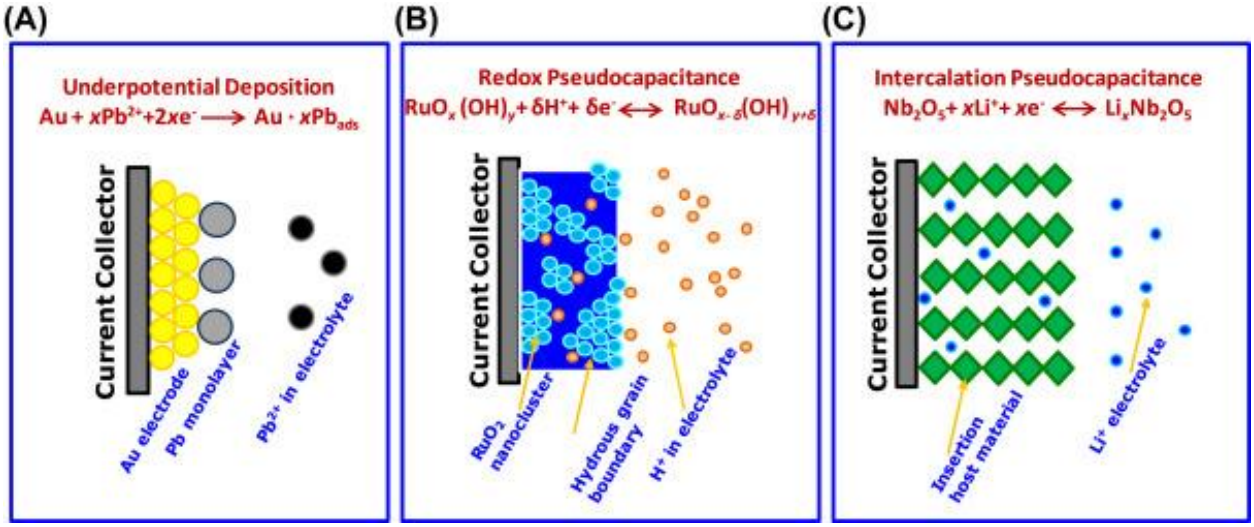

Figure 2-3: Mechanism of pseudo capacitance A) Underpotential deposition B) Redox Pseudo capacitance C) Intercalation pseudo capacitance [44]

2.3.1. Underpotential Pseudo capacitance

Ions in the electrolyte solution can form adsorbed monolayers of different metals on the electrode surface above the redox potential [47]. *Figure 2-3 shows that* the Pb^{2+} ions deposit on top of the gold electrode, forming a monolayer. Their voltage range is quite small due to the capacitance values being dependent on underpotential deposition and, therefore, low energy density. They have good charge-discharge kinetics and high-power density [48]. The charge transfer between the monolayer and the metal electrode is limited. The CVs of this process have highly reversible peaks, which are associated with different structures of monolayers. Early studies for UPD exist for polycrystalline electrode externals due to less difficulty in preparing and maintaining the crystal structure under controlled conditions [49].

2.3.2. Redox Pseudo capacitance

Redox reactions at the electrode surface are mainly due to surface redox pseudo capacitors [50]. The materials closely resembled carbon-based material based on their CVs and GCD, suggesting linear dependency of charge storage alongside the potential window; however, that charge storage does not depend on the double layer mechanism [51]. The materials that exhibit the in-build electrochemical properties can be called intrinsic pseudocapacitive materials [52]. Some materials, such as RuO_2, MnO_2, and Nb_2O_5, as well as other materials, are examples of redox pseudo-capacitors' properties.

2.4.1 Ruthenium Oxide

Ruthenium oxide is one of the most researched materials due to its advantages. It has a wider potential range, reversible redox reactions and a long cycle life [53]. RuO_2 is a conductive material with a rutile structure, and electrochemical stability [54]. Different reactions occur in acidic and alkaline medium electrolytes, representing pseudocapacitive behaviour. Due to its capacitive behaviour, RuO_2 has high redox properties and exhibits pseudocapacitive in aqueous solution [53]. The redox reaction follows:

$$RuO_2 + yH^+ + ne^- \leftrightarrow RuO_{2-x}(OH)_x \qquad \textit{Equation (2-1)}$$

RuO_2 and $RuO_{2-x(OH)}$ represent the higher and lower oxidation states, respectively [54], $RuO_2 \cdot nH_2O$ have four distinct properties that enable high capacitance and faradaic reactions. (1) the redox reaction happens due to the redox behaviour of Ru^{4+} cationic (2) conductivity allows faster electron transportation (3) the water in hydrated RuO_2 causes rapid and smooth proton transport (4) nano structuring causes high surface area, reducing diffusion distance. RuO_2 represents the faradaic charge transfer and has wider CVs inhibiting quasi-rectangular shape. A sequence of redox processes occurs, resulting in different oxidation of ruthenium Ru^{4+}, Ru^{3+} and Ru^{2+}, whose oxidative states contribute to its high capacitance. Due to its advantages, mesoporous RuO_2 has received attention from the industry for developing devices [55].

2.3.3 Intercalation pseudo capacitors

The intercalation pseudo capacitor mechanism allows charge storage in bulk material and performs electrochemical activity in nonaqueous systems [56]. Ions intercalate into tunnels in layered materials, causing faradic charge transfer without any structural change [53]. The intercalation of cations into transition metal oxide is diffusion-controlled [54]. Compared with EDLC, the charging mechanism for faradic reversible electrochemical reactions does not rely on surface and bulk

materials consumption [53]. Pseudocapacitive materials in nonaqueous electrolytes have the advantage of capacity in a wider potential range than aqueous solutions. For surface–controlled intercalation, there is growing interest in materials with higher diffusion coefficients and minimized phase transformation [54].

2.4. Transition metal oxides

Transition metal oxides (TMOs) have expanded immense attention due to their diversified applications related to their unique structure and properties. These TMOs have attracted most of their attention to the pseudo-capacitor electrodes because of their higher energy output than the EDLC materials [57]. Transition metal oxides inhibit different structures and characteristics. They are prominent choices for active materials for fabricating the electrodes in energy storage devices. It is also one of the leading nanomaterials groups for environmental industries [58]. TMOs have good structural, electrical, and electrochemical properties and variable oxidation states due to the incomplete d-subshell. Scaling the TMOs to their nanoscale capabilities has shown increased surface area. TMO electrodes are great candidates as energy storage systems [57]. TMOs have been studied extensively because of their low cost, environmental accessibility, and electrochemical stability for supercapacitors [57]. Transition metal oxides have represented large families of precursors for the development of nanomaterials. However, the performance of bulk metal oxides might not meet the requirements for applications [59].

TMOs with different structures and characteristics are promising choices of active materials for fabricating electrodes in energy storage devices [60]. In supercapacitors, metal oxides are commonly utilized due to their excellent capacitive performance [61]. Metal oxides, including MnO_2 [62], Fe_2O_3 [63], Bi_2O_3 [64], WO_3[65], and TMO nanostructures, have shown great potential in supercapacitors applications. Nanostructures are materials that have dimensions

between 1 to 100 nm. These are characterized into three morphologies: zero-dimension (0D, includes nanocrystals and nanoparticles), one-dimension (1D, which includes nanowires and nanotubes), two dimensions (2D includes nanoflakes and nanoplatelets) and three dimensions (3D, includes hollow, mesoporous structures) [66,67].

2.4.1. Titanium Dioxides based Sodium Hexa-Titanates

Titanium dioxide nanostructures can be considered as a potential electrode material in developing pseudocapacitive ES. Due to low cost, and environmental abundance. It has wide bandgap semiconductors in anatase, brookite and rutile phases. Nanostructures-based TiO_2 have low volume change and large surface area, causing easier intercalation or deintercalation of metal ions and diffusion short length. Many different TiO_2 nanostructures exist, such as nanowires, nanotubes, nanofibers and nanorods. The specific capacitance is lower than other materials due to electrical resistivity and low diffusion capacity [68]. Titanates-based nanowires can act as promising alternatives for supercapacitors for their open-layered structure and shorter diffusion paths for electrolytes [69].

Titania nanostructures offer unique properties, such as a well-defined structure with high electrical and chemical stabilities, making them suitable TMO candidate materials for long-lasting electrochemical capacitors and storage devices [70]. Titanium dioxide nanomaterials in layers have been thoroughly investigated for high retention of charge and cyclability performances [71]. Sodium titanates are compounds where the ratio of sodium to titanate changes the lattice structure and allows it to form a tunnel structure [72]. Due to their morphology, these layered structures can be a potential candidate for supercapacitors. They can store charges and possess shorter diffusion distances to reach the interlayer position. It was reported that sodium titanates could improve

charge-discharge cycles due to its structural tolerance during intercalation [73]. However, TMOs are inherently low-conductivity materials that prevent fast charge transfer electrochemical properties [74]. The recent literature has well-founded the idea that introducing oxygen vacancies within the lattice structures of TiO_2 nanostructures enhances the electrical and conductive properties of the material [75]. Oxygen vacancies were also reported to improve the pseudocapacitive behaviour [76]. Furthermore, introducing oxygen vacancies in lattice structures is also an innovative way to enhance material electrochemical performance. It creates electrochemical active sites, reduces material resistance, and improves kinetics [77]. Introducing oxygen vacancies into TiO_2 lattice structures has been shown to create Ti^{3+} sites from Ti^{4+} oxidative states on the surface, leading to the creation of oxygen vacancies [78]. *Table 2-2* shows the combination of TiO_2 material with different metal oxides.

Table 2-2: Specific capacitance of different combinations of metal oxide with titanium dioxide

Materials	Electrolyte	Specific Capacitance	Scan rate	References
TiO_2/MnO_2	Na_2SO_4	101 $mFcm^{-2}$	10mV/s	[79]
TiO_2 /NiO	NaOH	46.3 $mFcm^{-2}$	5mV/s	[80]
TiO_2 /MoO_3	Ammonium Fluoride	302 F/g	20mV/s	[81]
TiO_2/V_2O_5	$HClO_4$	220 F/g	50 mV/s	[82]
TiO_2 Nanowires	Na_2SO_4	121.5 $mFcm^{-2}$	1mV/s	[83]

2.4.2. Cobalt Oxide Nanoparticles

Cobalt oxide (Co_3O_4) is an essential metal oxide that has gained attention and has been studied for pseudocapacitive behaviour in applications [84]. The p-type semiconductor in the Co_3O_4 showed enhanced electroactive sites suitable for electrochemical capacitors [85]. Co_3O_4 has been studied for many years as an active material for supercapacitors and charge storage by faradic and non-

faradic processes. Cobalt oxides have enhanced surface area and better chemical stability and properties associated with cobalt oxides-based materials and find their applications in their supercapacitors [86]. The electrochemical properties of cobalt oxides depend on the materials' structural morphology and the metal's electronic states. To improve charge storage performance, several strategies have been employed to create various forms of cobalt oxide nanocomposites [87]. 2D cobalt oxide nanostructures have been designed for larger surface areas and reduced distances for ion diffusion compared to bulk materials. Co_3O_4 nanorod arrays, nanowires and hollow coral-shaped Co_3O_4 nanostructures showed excellent electrochemical performance [88]. Many experimental factors have affected the nanostructure's pore dimension and morphology, impacting electrochemical performance regarding pH temperature, precursor, and concentration. pH and solvent polarity influence the regulation of precursor nanostructures. As suggested by Wei et al., they have synthesized ultrathin nano meshes through precursor thermal treatment of ultrathin metal-organic framework nanosheets with uniform pore sized and oxygen vacancies, which provided advanced nanomaterial and enhanced the electrochemical properties. [89]. Many experimental optimal conditions are being researched to successfully grow nanostructures for better faradic redox reactions [90].

2.5. References

[1] A. Basit, M. G. Mohamed, M. Ejaz, B. Xuan Su, H. Manzoor, and S.-W. Kuo, "Boosting Supercapacitor Energy Storage Using Microporous Carbon Derived from an Octavinylsilsesquioxane and Fluorenone-Linked Porous Hybrid Polymer," *ACS Appl. Energy Mater.*, vol. 7, no. 17, pp. 7505–7516, Sep. 2024, doi: 10.1021/acsaem.4c01796.

[2] O. Z. Sharaf and M. F. Orhan, "An overview of fuel cell technology: Fundamentals and applications," *Renewable and Sustainable Energy Reviews*, vol. 32, pp. 810–853, Apr. 2014, doi: 10.1016/j.rser.2014.01.012.

[3] "Early Market Applications for Fuel Cell Technologies," Energy.gov. Accessed: Nov. 27, 2024. [Online]. Available: https://www.energy.gov/eere/fuelcells/early-market-applications-fuel-cell-technologies

[4] A. Burke, "R&D considerations for the performance and application of electrochemical capacitors," *Electrochimica Acta*, vol. 53, no. 3, pp. 1083–1091, Dec. 2007, doi: 10.1016/j.electacta.2007.01.011.

[5] P. Simon and Y. Gogotsi, "Perspectives for electrochemical capacitors and related devices," *Nat. Mater.*, vol. 19, no. 11, pp. 1151–1163, Nov. 2020, doi: 10.1038/s41563-020-0747-z.

[6] J. Sun, B. Luo, and H. Li, "A Review on the Conventional Capacitors, Supercapacitors, and Emerging Hybrid Ion Capacitors: Past, Present, and Future," *Advanced Energy and Sustainability Research*, vol. 3, no. 6, p. 2100191, 2022, doi: 10.1002/aesr.202100191.

[7] Z. Lin *et al.*, "Materials for supercapacitors: When Li-ion battery power is not enough," *Materials Today*, vol. 21, no. 4, pp. 419–436, May 2018, doi: 10.1016/j.mattod.2018.01.035.

[8] P. Simon and Y. Gogotsi, "Materials for electrochemical capacitors," *Nature Mater*, vol. 7, no. 11, pp. 845–854, Nov. 2008, doi: 10.1038/nmat2297.

[9] M. Salanne *et al.*, "Efficient storage mechanisms for building better supercapacitors," *Nat Energy*, vol. 1, no. 6, pp. 1–10, May 2016, doi: 10.1038/nenergy.2016.70.

[10] P. Sinha and K. K. Kar, "Introduction to Supercapacitors," in *Handbook of Nanocomposite Supercapacitor Materials II: Performance*, K. K. Kar, Ed., Cham: Springer International Publishing, 2020, pp. 1–28. doi: 10.1007/978-3-030-52359-6_1.

[11] C. D. Lokhande, D. P. Dubal, and O.-S. Joo, "Metal oxide thin film based supercapacitors," *Current Applied Physics*, vol. 11, no. 3, pp. 255–270, May 2011, doi: 10.1016/j.cap.2010.12.001.

[12] S. M. Jadhav *et al.*, "Cobalt-Doped Manganese Dioxide Hierarchical Nanostructures for Enhancing Pseudocapacitive Properties," *ACS Omega*, vol. 6, no. 8, pp. 5717–5729, Mar. 2021, doi: 10.1021/acsomega.0c06150.

[13] R. Kötz and M. Carlen, "Principles and applications of electrochemical capacitors," *Electrochimica Acta*, vol. 45, no. 15, pp. 2483–2498, May 2000, doi: 10.1016/S0013-4686(00)00354-6.

[14] B.-A. Mei, O. Munteshari, J. Lau, B. Dunn, and L. Pilon, "Physical Interpretations of Nyquist Plots for EDLC Electrodes and Devices," *J. Phys. Chem. C*, vol. 122, no. 1, pp. 194–206, Jan. 2018, doi: 10.1021/acs.jpcc.7b10582.

[15] B. Fang and L. Binder, "A Novel Carbon Electrode Material for Highly Improved EDLC Performance," *J. Phys. Chem. B*, vol. 110, no. 15, pp. 7877–7882, Apr. 2006, doi: 10.1021/jp060110d.

[16] X. Zhao *et al.*, "Two-dimensional Spinel Structured Co-based Materials for High Performance Supercapacitors: A Critical Review," *Chemical Engineering Journal*, vol. 387, p. 124081, May 2020, doi: 10.1016/j.cej.2020.124081.
[17] Q. T. Qu, B. Wang, L. C. Yang, Y. Shi, S. Tian, and Y. P. Wu, "Study on electrochemical performance of activated carbon in aqueous Li2SO4, Na2SO4 and K2SO4 electrolytes," *Electrochemistry Communications*, vol. 10, no. 10, pp. 1652–1655, Oct. 2008, doi: 10.1016/j.elecom.2008.08.020.
[18] L. G. H. Staaf, P. Lundgren, and P. Enoksson, "Present and future supercapacitor carbon electrode materials for improved energy storage used in intelligent wireless sensor systems," *Nano Energy*, vol. 9, pp. 128–141, Oct. 2014, doi: 10.1016/j.nanoen.2014.06.028.
[19] S. L. Revo, I. M. Budzulyak, B. I. Rachiy, and M. M. Kuzishin, "Electrode material for supercapacitors based on nanostructured carbon," *Surf. Engin. Appl.Electrochem.*, vol. 49, no. 1, pp. 68–72, Feb. 2013, doi: 10.3103/S1068375513010122.
[20] G. C. Gschwend and H. H. Girault, "Discrete Helmholtz model: a single layer of correlated counter-ions. Metal oxides and silica interfaces, ion-exchange and biological membranes," *Chemical Science*, vol. 11, no. 38, pp. 10304–10312, 2020, doi: 10.1039/D0SC03748F.
[21] Z. Zhai *et al.*, "A review of carbon materials for supercapacitors," *Materials & Design*, vol. 221, p. 111017, Sep. 2022, doi: 10.1016/j.matdes.2022.111017.
[22] K. Makgopa *et al.*, "Nanostructured Carbon-Based Electrode Materials for Supercapacitor Applications," in *Carbon Related Materials: Commemoration for Nobel Laureate Professor Suzuki Special Symposium at IUMRS-ICAM2017*, S. Kaneko, M. Aono, A. Pruna, M. Can, P. Mele, M. Ertugrul, and T. Endo, Eds., Singapore: Springer, 2021, pp. 317–355. doi: 10.1007/978-981-15-7610-2_14.
[23] R. A. Geioushy, S. Y. Attia, S. G. Mohamed, H. Li, and O. A. Fouad, "High-performance electrode materials for supercapacitor applications using Ni-catalyzed carbon nanostructures derived from biomass waste materials," *Journal of Energy Storage*, vol. 48, p. 104034, Apr. 2022, doi: 10.1016/j.est.2022.104034.
[24] G. F. L. Pereira, E. E. Fileti, and L. J. A. Siqueira, "Comparing Graphite and Graphene Oxide Supercapacitors with a Constant Potential Model," *J. Phys. Chem. C*, vol. 125, no. 4, pp. 2318–2326, Feb. 2021, doi: 10.1021/acs.jpcc.0c10347.
[25] C. Lei, N. Amini, F. Markoulidis, P. Wilson, S. Tennison, and C. Lekakou, "Activated carbon from phenolic resin with controlled mesoporosity for an electric double-layer capacitor (EDLC)," *J. Mater. Chem. A*, vol. 1, no. 19, pp. 6037–6042, Apr. 2013, doi: 10.1039/C3TA01638B.
[26] B. Xu *et al.*, "Highly mesoporous and high surface area carbon: A high capacitance electrode material for EDLCs with various electrolytes," *Electrochemistry Communications*, vol. 10, no. 5, pp. 795–797, May 2008, doi: 10.1016/j.elecom.2008.02.033.
[27] M. H. Hamsan, S. B. Aziz, M. F. Z. Kadir, M. A. Brza, and W. O. Karim, "The study of EDLC device fabricated from plasticized magnesium ion conducting chitosan based polymer electrolyte," *Polymer Testing*, vol. 90, p. 106714, Oct. 2020, doi: 10.1016/j.polymertesting.2020.106714.
[28] R. Taslim, A. Apriwandi, and E. Taer, "Novel Moringa oleifera Leaves 3D Porous Carbon-Based Electrode Material as a High-Performance EDLC Supercapacitor," *ACS Omega*, vol. 7, no. 41, pp. 36489–36502, Oct. 2022, doi: 10.1021/acsomega.2c04301.

[29] X. You, M. Misra, S. Gregori, and A. K. Mohanty, "Preparation of an Electric Double Layer Capacitor (EDLC) Using Miscanthus-Derived Biocarbon," *ACS Sustainable Chem. Eng.*, vol. 6, no. 1, pp. 318–324, Jan. 2018, doi: 10.1021/acssuschemeng.7b02563.
[30] R. Chen, M. Yu, R. P. Sahu, I. K. Puri, and I. Zhitomirsky, "The Development of Pseudocapacitor Electrodes and Devices with High Active Mass Loading," *Advanced Energy Materials*, vol. 10, no. 20, p. 1903848, 2020, doi: 10.1002/aenm.201903848.
[31] C. Choi *et al.*, "Achieving high energy density and high power density with pseudocapacitive materials," *Nat Rev Mater*, vol. 5, no. 1, pp. 5–19, Jan. 2020, doi: 10.1038/s41578-019-0142-z.
[32] N. R. Chodankar *et al.*, "True Meaning of Pseudocapacitors and Their Performance Metrics: Asymmetric versus Hybrid Supercapacitors," *Small*, vol. 16, no. 37, p. 2002806, 2020, doi: 10.1002/smll.202002806.
[33] J. Wang, X. Zhang, Z. Li, Y. Ma, and L. Ma, "Recent progress of biomass-derived carbon materials for supercapacitors," *Journal of Power Sources*, vol. 451, p. 227794, Mar. 2020, doi: 10.1016/j.jpowsour.2020.227794.
[34] N. Liu, J. Shen, and D. Liu, "Activated high specific surface area carbon aerogels for EDLCs," *Microporous and Mesoporous Materials*, vol. 167, pp. 176–181, Feb. 2013, doi: 10.1016/j.micromeso.2012.09.009.
[35] C. Lei, N. Amini, F. Markoulidis, P. Wilson, S. Tennison, and C. Lekakou, "Activated carbon from phenolic resin with controlled mesoporosity for an electric double-layer capacitor (EDLC)," *J. Mater. Chem. A*, vol. 1, no. 19, pp. 6037–6042, Apr. 2013, doi: 10.1039/C3TA01638B.
[36] B. Xu *et al.*, "Highly mesoporous and high surface area carbon: A high capacitance electrode material for EDLCs with various electrolytes," *Electrochemistry Communications*, vol. 10, no. 5, pp. 795–797, May 2008, doi: 10.1016/j.elecom.2008.02.033.
[37] M. H. Hamsan, S. B. Aziz, M. F. Z. Kadir, M. A. Brza, and W. O. Karim, "The study of EDLC device fabricated from plasticized magnesium ion conducting chitosan based polymer electrolyte," *Polymer Testing*, vol. 90, p. 106714, Oct. 2020, doi: 10.1016/j.polymertesting.2020.106714.
[38] Z. Liu, Z. Zhu, J. Dai, and Y. Yan, "Waste Biomass Based-Activated Carbons Derived from Soybean Pods as Electrode Materials for High-Performance Supercapacitors", doi: 10.1002/slct.201800609.
[39] X. You, M. Misra, S. Gregori, and A. K. Mohanty, "Preparation of an Electric Double Layer Capacitor (EDLC) Using Miscanthus-Derived Biocarbon," *ACS Sustainable Chem. Eng.*, vol. 6, no. 1, pp. 318–324, Jan. 2018, doi: 10.1021/acssuschemeng.7b02563.
[40] A. Kumar, H. K. Rathore, D. Sarkar, and A. Shukla, "Nanoarchitectured transition metal oxides and their composites for supercapacitors," *Electrochemical Science Advances*, vol. 2, no. 6, p. e2100187, 2022, doi: 10.1002/elsa.202100187.
[41] A. González, E. Goikolea, J. A. Barrena, and R. Mysyk, "Review on supercapacitors: Technologies and materials," *Renewable and Sustainable Energy Reviews*, vol. 58, pp. 1189–1206, May 2016, doi: 10.1016/j.rser.2015.12.249.
[42] J. Liu *et al.*, "Advanced Energy Storage Devices: Basic Principles, Analytical Methods, and Rational Materials Design," *Advanced Science*, vol. 5, no. 1, p. 1700322, 2018, doi: 10.1002/advs.201700322.

[43] J. Meng *et al.*, "Identification of Phase Control of Carbon-Confined Nb2O5 Nanoparticles toward High-Performance Lithium Storage," *Advanced Energy Materials*, vol. 9, no. 18, p. 1802695, 2019, doi: 10.1002/aenm.201802695.

[44] M. Sarno, "Nanotechnology in energy storage: the supercapacitors," in *Studies in Surface Science and Catalysis*, vol. 179, Elsevier, 2020, pp. 431–458. doi: 10.1016/B978-0-444-64337-7.00022-7.

[45] E. Herrero, L. J. Buller, and H. D. Abruña, "Underpotential Deposition at Single Crystal Surfaces of Au, Pt, Ag and Other Materials," *Chem. Rev.*, vol. 101, no. 7, pp. 1897–1930, Jul. 2001, doi: 10.1021/cr9600363.

[46] J. Cao and W. Wang, "Pseudocapacitive Materials," in *Handbook of Energy Materials*, R. Gupta, Ed., Singapore: Springer Nature, 2022, pp. 1–29. doi: 10.1007/978-981-16-4480-1_24-1.

[47] S. Fleischmann *et al.*, "Pseudocapacitance: From Fundamental Understanding to High Power Energy Storage Materials," *Chem. Rev.*, vol. 120, no. 14, pp. 6738–6782, Jul. 2020, doi: 10.1021/acs.chemrev.0c00170.

[48] S. J. Panchu, K. Raju, and H. C. Swart, "Emerging Two–Dimensional Intercalation Pseudocapacitive Electrodes for Supercapacitors," *ChemElectroChem*, vol. 11, no. 15, p. e202300810, 2024, doi: 10.1002/celc.202300810.

[49] B. Babu, P. Simon, and A. Balducci, "Fast Charging Materials for High Power Applications," *Advanced Energy Materials*, vol. 10, no. 29, p. 2001128, 2020, doi: 10.1002/aenm.202001128.

[50] F. Bibi, O. Gerard, A. J. Khan, M. Khalid, and A. Numan, "3 - Categories of pseudocapacitor: intrinsic, extrinsic, and intercalation materials," in *Supercapacitors*, S. G. Krishnan, H. D. Pham, and D. P. Dubal, Eds., Elsevier, 2024, pp. 45–70. doi: 10.1016/B978-0-443-15478-2.00005-X.

[51] P. Bhojane, "Recent advances and fundamentals of Pseudocapacitors: Materials, mechanism, and its understanding," *Journal of Energy Storage*, vol. 45, p. 103654, Jan. 2022, doi: 10.1016/j.est.2021.103654.

[52] S. Jayakumar, P. C. Santhosh, M. M. Mohideen, and A. V. Radhamani, "A comprehensive review of metal oxides (RuO2, Co3O4, MnO2 and NiO) for supercapacitor applications and global market trends," *Journal of Alloys and Compounds*, vol. 976, p. 173170, Mar. 2024, doi: 10.1016/j.jallcom.2023.173170.

[53] D. Rochefort and A.-L. Pont, "Pseudocapacitive behaviour of RuO2 in a proton exchange ionic liquid," *Electrochemistry Communications*, vol. 8, no. 9, pp. 1539–1543, Sep. 2006, doi: 10.1016/j.elecom.2006.06.032.

[54] M. D. Levi and D. Aurbach, "Frumkin intercalation isotherm — a tool for the description of lithium insertion into host materials: a review," *Electrochimica Acta*, vol. 45, no. 1, pp. 167–185, Sep. 1999, doi: 10.1016/S0013-4686(99)00202-9.

[55] J. García-Cañadas, I. Mora-Seró, F. Fabregat-Santiago, J. Bisquert, and G. Garcia-Belmonte, "Analysis of cyclic voltammograms of electrochromic *a*-WO3 films from voltage-dependent equilibrium capacitance measurements," *Journal of Electroanalytical Chemistry*, vol. 565, no. 2, pp. 329–334, Apr. 2004, doi: 10.1016/j.jelechem.2003.10.027.

[56] X. Han *et al.*, "Intercalation pseudocapacitive electrochemistry of Nb-based oxides for fast charging of lithium-ion batteries," *Nano Energy*, vol. 81, p. 105635, Mar. 2021, doi: 10.1016/j.nanoen.2020.105635.

[57] A. Kumar, H. K. Rathore, D. Sarkar, and A. Shukla, "Nanoarchitectured transition metal oxides and their composites for supercapacitors," *Electrochemical Science Advances*, vol. 2, no. 6, p. e2100187, 2022, doi: 10.1002/elsa.202100187.
[58] Lichchhavi, A. Kanwade, and P. M. Shirage, "A review on synergy of transition metal oxide nanostructured materials: Effective and coherent choice for supercapacitor electrodes," *Journal of Energy Storage*, vol. 55, p. 105692, Nov. 2022, doi: 10.1016/j.est.2022.105692.
[59] C. Chen, Y. Fan, J. Gu, L. Wu, S. Passerini, and L. Mai, "One-dimensional nanomaterials for energy storage," *J. Phys. D: Appl. Phys.*, vol. 51, no. 11, p. 113002, Mar. 2018, doi: 10.1088/1361-6463/aaa98d.
[60] T. Guo, M.-S. Yao, Y.-H. Lin, and C.-W. Nan, "A comprehensive review on synthesis methods for transition-metal oxide nanostructures," *CrystEngComm*, vol. 17, no. 19, pp. 3551–3585, May 2015, doi: 10.1039/C5CE00034C.
[61] C. An, Y. Zhang, H. Guo, and Y. Wang, "Metal oxide-based supercapacitors: progress and prospectives," *Nanoscale Adv.*, vol. 1, no. 12, pp. 4644–4658, Dec. 2019, doi: 10.1039/C9NA00543A.
[62] K. Makgopa *et al.*, "A high-rate aqueous symmetric pseudocapacitor based on highly graphitized onion-like carbon/birnessite-type manganese oxide nanohybrids," *Journal of Materials Chemistry A*, vol. 3, no. 7, pp. 3480–3490, 2015, doi: 10.1039/C4TA06715K.
[63] G. Zhou *et al.*, "A nanosized Fe2O3 decorated single-walled carbon nanotube membrane as a high-performance flexible anode for lithium ion batteries," *J. Mater. Chem.*, vol. 22, no. 34, pp. 17942–17946, Aug. 2012, doi: 10.1039/C2JM32893C.
[64] T. P. Gujar, V. R. Shinde, C. D. Lokhande, and S.-H. Han, "Electrosynthesis of Bi2O3 thin films and their use in electrochemical supercapacitors," *Journal of Power Sources*, vol. 161, no. 2, pp. 1479–1485, Oct. 2006, doi: 10.1016/j.jpowsour.2006.05.036.
[65] S. K. Deb, "Opportunities and challenges in science and technology of WO3 for electrochromic and related applications," *Solar Energy Materials and Solar Cells*, vol. 92, no. 2, pp. 245–258, Feb. 2008, doi: 10.1016/j.solmat.2007.01.026.
[66] A. Jain *et al.*, "Vanadium oxide nanorods as an electrode material for solid state supercapacitor," *Sci Rep*, vol. 12, no. 1, Art. no. 1, Dec. 2022, doi: 10.1038/s41598-022-25707-z.
[67] Y. Ma *et al.*, "Recent advances in transition metal oxides with different dimensions as electrodes for high-performance supercapacitors," *Adv Compos Hybrid Mater*, vol. 4, no. 4, pp. 906–924, Dec. 2021, doi: 10.1007/s42114-021-00358-2.
[68] H. R. Barai, Md. M. Rahman, and S. W. Joo, "Template-free synthesis of two-dimensional titania/titanate nanosheets as electrodes for high-performance supercapacitor applications," *Journal of Power Sources*, vol. 372, pp. 227–234, Dec. 2017, doi: 10.1016/j.jpowsour.2017.10.076.
[69] W. Zhou *et al.*, "Enhanced Performance of Layered Titanate Nanowire-Based Supercapacitor Electrodes by Nickel Ion Exchange," *ACS Appl. Mater. Interfaces*, vol. 6, no. 6, pp. 4578–4586, Mar. 2014, doi: 10.1021/am500421r.
[70] M. Ates, Y. Bayrak, O. Yoruk, and S. Caliskan, "Reduced graphene oxide/Titanium oxide nanocomposite synthesis via microwave-assisted method and supercapacitor behaviors," *Journal of Alloys and Compounds*, vol. 728, pp. 541–551, Dec. 2017, doi: 10.1016/j.jallcom.2017.08.298.

[71] M. Liu *et al.*, "Introducing oxygen vacancies for improving the electrochemical performance of Co9S8@NiCo-LDH nanotube arrays in flexible all-solid battery-capacitor hybrid supercapacitors," *Energy*, vol. 238, p. 121767, Jan. 2022, doi: 10.1016/j.energy.2021.121767.
[72] M. G. Kim *et al.*, "Effects of Calcination Temperature on the Phase Composition, Photocatalytic Degradation, and Virucidal Activities of TiO2 Nanoparticles," *ACS Omega*, vol. 6, no. 16, pp. 10668–10678, Apr. 2021, doi: 10.1021/acsomega.1c00043.
[73] X. Zheng *et al.*, "Understanding the structural and chemical evolution of layered potassium titanates for sodium ion batteries," *Energy Storage Materials*, vol. 25, pp. 502–509, Mar. 2020, doi: 10.1016/j.ensm.2019.09.032.
[74] H. Zhang, X. P. Gao, G. R. Li, T. Y. Yan, and H. Y. Zhu, "Electrochemical lithium storage of sodium titanate nanotubes and nanorods," *Electrochimica Acta*, vol. 53, no. 24, pp. 7061–7068, Oct. 2008, doi: 10.1016/j.electacta.2008.05.036.
[75] W. Zhou *et al.*, "Enhanced Performance of Layered Titanate Nanowire-Based Supercapacitor Electrodes by Nickel Ion Exchange," *ACS Appl. Mater. Interfaces*, vol. 6, no. 6, pp. 4578–4586, Mar. 2014, doi: 10.1021/am500421r.
[76] M. Xiao *et al.*, "Enhancement of electrochemical properties of electrodes for high performance supercapacitors by electrodeposition of CoSe on hydrothermally prepared CuCo2O4," *Journal of Alloys and Compounds*, vol. 968, p. 172199, Dec. 2023, doi: 10.1016/j.jallcom.2023.172199.
[77] V. S. Drozd *et al.*, "Oxygen vacancies in nano-sized TiO2 anatase nanoparticles," *Solid State Ionics*, vol. 339, p. 115009, Oct. 2019, doi: 10.1016/j.ssi.2019.115009.
[78] Z. Hu *et al.*, "Building oxygen-vacancy in Co3O4−x nanocrystal towards ultrahigh pseudocapacitance," *Journal of Alloys and Compounds*, vol. 929, p. 167299, Dec. 2022, doi: 10.1016/j.jallcom.2022.167299.
[79] R. Kumar, B. K. Singh, A. Soam, S. Parida, V. Sahajwalla, and P. Bhargava, "In situ carbon-supported titanium dioxide (ICS-TiO2) as an electrode material for high performance supercapacitors," *Nanoscale Adv.*, vol. 2, no. 6, pp. 2376–2386, Jun. 2020, doi: 10.1039/D0NA00014K.
[80] H. Zhou and Y. Zhang, "Enhanced electrochemical performance of manganese dioxide spheres deposited on a titanium dioxide nanotube arrays substrate," *Journal of Power Sources*, vol. 272, pp. 866–879, Dec. 2014, doi: 10.1016/j.jpowsour.2014.09.030.
[81] Y. Xie, C. Huang, L. Zhou, Y. Liu, and H. Huang, "Supercapacitor application of nickel oxide–titania nanocomposites," *Composites Science and Technology*, vol. 69, no. 13, pp. 2108–2114, Oct. 2009, doi: 10.1016/j.compscitech.2009.01.018.
[82] R. S. Ray, B. Sarma, and M. Misra, "Random shaped ZnO supported on a porous substrate as supercapacitor," *Materials Letters*, vol. 155, pp. 102–105, Sep. 2015, doi: 10.1016/j.matlet.2015.04.010.
[83] Y. Yang, D. Kim, M. Yang, and P. Schmuki, "Vertically aligned mixed V2O5–TiO2 nanotube arrays for supercapacitor applications," *Chem. Commun.*, vol. 47, no. 27, pp. 7746–7748, Jun. 2011, doi: 10.1039/C1CC11811K.
[84] W. Guo *et al.*, "TiO2 Nanowire Arrays on Titanium Substrate as a Novel Binder-free Negative Electrode for Asymmetric Supercapacitor," *Electrochimica Acta*, vol. 229, pp. 197–207, Mar. 2017, doi: 10.1016/j.electacta.2017.01.135.

[85] F. Liu, H. Su, L. Jin, H. Zhang, X. Chu, and W. Yang, "Facile synthesis of ultrafine cobalt oxide nanoparticles for high-performance supercapacitors," *Journal of Colloid and Interface Science*, vol. 505, pp. 796–804, Nov. 2017, doi: 10.1016/j.jcis.2017.06.058.
[86] M. A. A. Mohd Abdah, N. H. N. Azman, S. Kulandaivalu, and Y. Sulaiman, "Review of the use of transition-metal-oxide and conducting polymer-based fibres for high-performance supercapacitors," *Materials & Design*, vol. 186, p. 108199, Jan. 2020, doi: 10.1016/j.matdes.2019.108199.
[87] S. Veeresh *et al.*, "Graphene oxide/cobalt oxide nanocomposite for high-performance electrode for supercapacitor application," *Journal of Energy Storage*, vol. 52, p. 104715, Aug. 2022, doi: 10.1016/j.est.2022.104715.
[88] X. Zhao *et al.*, "Two-dimensional Spinel Structured Co-based Materials for High Performance Supercapacitors: A Critical Review," *Chemical Engineering Journal*, vol. 387, p. 124081, May 2020, doi: 10.1016/j.cej.2020.124081.
[89] G. Wei, Z. Zhou, X. Zhao, W. Zhang, and C. An, "Ultrathin Metal–Organic Framework Nanosheet-Derived Ultrathin Co_3O_4 Nanomeshes with Robust Oxygen-Evolving Performance and Asymmetric Supercapacitors," *ACS Appl. Mater. Interfaces*, vol. 10, no. 28, pp. 23721–23730, Jul. 2018, doi: 10.1021/acsami.8b04026.
[90] T. Nguyen and M. de F. Montemor, "Metal Oxide and Hydroxide–Based Aqueous Supercapacitors: From Charge Storage Mechanisms and Functional Electrode Engineering to Need-Tailored Devices," *Advanced Science*, vol. 6, no. 9, p. 1801797, 2019, doi: 10.1002/advs.201801797.

Chapter 3: Sodium Hexa-titanate nanocomposites modified with trace amounts of ruthenium for an enhanced supercapacitance

3.1. Introduction

Supercapacitors are a combination of electric double layer (EDL) and faradaic mechanisms, which allows them to have high power densities and long-life cycles, but their energy densities are relatively low [1]. In the recent past, research of TMO nanostructures has been geared towards enhancing supercapacitors for high energy densities. This is because TMOs possess high pseudo-capacitance due to weakly attached surface ions, which can further enhance the energy density of ECSCs [2,3].

In this study, a facile two-step process has been developed to synthesize or grow $Na_2Ti_6O_{13}$ nanocomposites on a Ti metal substrate surface using a hydrothermal process. Although titanium-layered materials such as sodium and potassium titanates have been implemented for sodium-ion batteries' anode applications, there has been no research on sodium titanate nanowires for supercapacitor applications till date. Then oxygen vacancies were successfully introduced into the lattice structure of the $Na_2Ti_6O_{13}$ nanocomposites, which showed an observable increase in its specific capacitance (C_{sp}). Further, to enhance the C_{sp}, trace amounts of Ru was coated on the surface of the Ti / $Na_2Ti_6O_{13}$ nanocomposites coupled with oxygen reduction procedure, which led the enhanced C_{sp}.

3.2. Experimental Details

3.2.1 Materials and Equipment:

Highly pure (99%) Titanium (Ti) plate foil (Grade 2) were purchased from McMaster-Carr and rinsed with ultrapure (Milli-Q water). Chemicals like sodium hydroxide (NaOH), sulfuric acid (H_2SO_4), and 18% hydrochloric acid (HCl) were purchased from Sigma Aldrich. Hexaamineruthenium (III) Chloride was purchased from Thermo Scientific. The electrochemical cell, Ag/AgCl reference electrode and platinum wire counter electrodes were purchased from BASi research products. Hexaamineruthenium (III) Chloride was prepared by adding 0.1 µg into isopropyl alcohol and sonicate for 10 minutes to prepare the 1mM stock solutions and diluted by 10-fold to prepare 0.1mM of Hexaamineruthenium (III) Chloride solution. All the electrochemical experiments were conducted using the PalmSens4 potentiostat. Fresh stock solutions and electrodes were prepared when performing each experiment to achieve the most accurate results.

3.2.2. Fabrication procedure:

3.2.2.1. Hydrothermal process and annealing:

Ti plates of 1 cm^2 area and a thickness of 0.25 mm were cut from a larger metal plate. These Ti plates or electrodes were cleaned by sonification in acetone and deionized water for about 5 mins. They were then etched by being immersed in 18% HCL boiled above 80 °C for 15 mins. The etched electrodes were washed and stored in deionized water for further use. Growth of $Na_2Ti_6O_{13}$ nanostructures directly on the etched Ti substrate were synthesized via hydrothermal process in a Teflon lined hydrothermal vessel (of 100 mL capacity) containing 40 mL of 1 M NaOH at 200 °C for 24 hrs. After the hydrothermal treatment, the electrodes were washed several times with ultrapure water and were subsequently annealed at 150 °C, 350 °C and 650 °C, respectively, for 3

h using a muffle furnace (Gilson company model: MF-2A) to obtain Ti/$Na_2Ti_6O_{13}$ nanocomposites.

3.2.2.2. Modification of Ti/$Na_2Ti_6O_{13}$ nanocomposites with ruthenium

The synthesized Ti/$Na_2Ti_6O_{13}$ nanocomposites were modified by trace amounts of Ru, with loading amount 0.4 µg cm^{-2} to synthesize modified Ru-Ti/$Na_2Ti_6O_{13}$. A drop casting method was employed for Ru modification of Ti/$Na_2Ti_6O_{13}$, where a 40 µL of 0.1 mM of Hexa-amine ruthenium (III) Chloride in isopropyl alcohol was deposited on the surface of Ti/$Na_2Ti_6O_{13}$ nanocomposites. As prepared Ru-Ti/$Na_2Ti_6O_{13}$ electrodes were annealed for 3 h at temperatures of 150 °C, 350 °C and 650 °C, respectively.

3.2.2.3. Electrochemical reduction (EC) treatment post annealing

To induce oxygen vacancies into the lattice structures of Ti/$Na_2Ti_6O_{13}$ and Ru- Ti/$Na_2Ti_6O_{13}$ nanocomposites, a facile electrochemical reduction (EC) treatment was employed. The EC treatment was performed in a 0.1 M H_2SO_4 solution under a high applied reducing current of -1 mA cm^2 for 5 min using a chronopotentiometry technique in a three-electrode system, where Ag/AgCl was used as reference electrode and Pt wire (of approx. 10.0 cm^2 surface are) was used as the anode or counter electrode.

3.2.3. Characterization:

Surface morphologies of Ti/$Na_2Ti_6O_{13}$ nanocomposites and Ru-Ti/$Na_2Ti_6O_{13}$ nanocomposites were characterized by a Quattro S environmental scanning electron microscope (ESEM) coupled with energy dispersive X-ray spectroscopy (EDS). The crystalline phase of the synthesized samples was investigated using a D8 discover machine at the McMaster Analytical X-ray diffraction facility (MAX) (XRD, Bruker). The investigation of electrode oxidation states was done through quantum imaging and scanning X-ray photoelectron spectrometer (XPS, PHI

electronics). All mass for chemicals and electrodes were measured using a VWR analytical balance.

3.2.4. Electrochemical studies

The electrochemical experiments were performed using PalmSens PSTrace Software. An Ag/AgCl (3 M KCl) electrode was used as a reference electrode, and a platinum (Pt) wire electrode with an approximate surface area of about 10.0 cm^2 was used as a counter electrode. Data analysis and image configuration were performed using the Origin 8.5 software (OriginLab, United States). The specific capacitances (C_{sp}) values were calculated for pristine Ti/$Na_2Ti_6O_{13}$ and for Ru-Ti/$Na_2Ti_6O_{13}$ (F cm^{-2} g^{-1}) from CV curves and GCD curves according to equations 1 and 2 respectively.

$$C_{sp} = \frac{\int_{v_1}^{v_2} I(V)\, dV}{mv(V_2 - V_1)}, \qquad \text{--- Equation. (3-1)}$$

where, $\int_{v_1}^{v_2} I(V)$ is the integrated CV loop area, dV is operational potential window (V), v is applied scan rate (V s^{-1}), m (g) is loading mass of Ru on electrode [4].

$$C_{sp} = \frac{I\,(\frac{\mu A}{cm^2}) \times \Delta t}{m\,(\mu g) \times \Delta V}, \qquad \text{--- Equation. (3-2)}$$

where, I (μA) is the applied current range, Δt is the discharge time in (s), m (μg) is loading mass on electrode and ΔV is the operated potential window to discharge (V) [5]. Further, the columbic efficiency is calculated through equation 3.

$$\eta = \frac{t_D}{t_C} \times 100\% \qquad \text{--- Equation. (3-3)}$$

where, t_D' represents the discharging time, and t_C is the charging time of electrode [6].

3.3. Results and Discussion

3.3.1. Characterization of $Na_2Ti_6O_{13}$ and Ru-$Na_2Ti_6O_{13}$

A hydrothermal method was employed to synthesize the $Na_2Ti_6O_{13}$ nanowires and nanoplate structures (nanocomposites) on the surface of a Ti metal plate. The nanocomposite morphology of sodium hexa-titanates ($Na_2Ti_6O_{13}$) was investigated through an environmental scanning electron microscope (ESEM). *Figure 3-1 (a)* shows long and thin $Na_2Ti_6O_{13}$ nanowire structure and flat nanoplates that are uniformly spread on the entire Ti surface with the nanowire's average diameter measuring at 34.808 nm. *Figure 3-1(b)* shows the Ti/$Na_2Ti_6O_{13}$ nanocomposites modified with Ru particles drop casting with loading amount of 0.4 µg cm^{-2}, revealing discernable morphological changes in terms of cluster formation of nanowires after annealing at 650 °C.

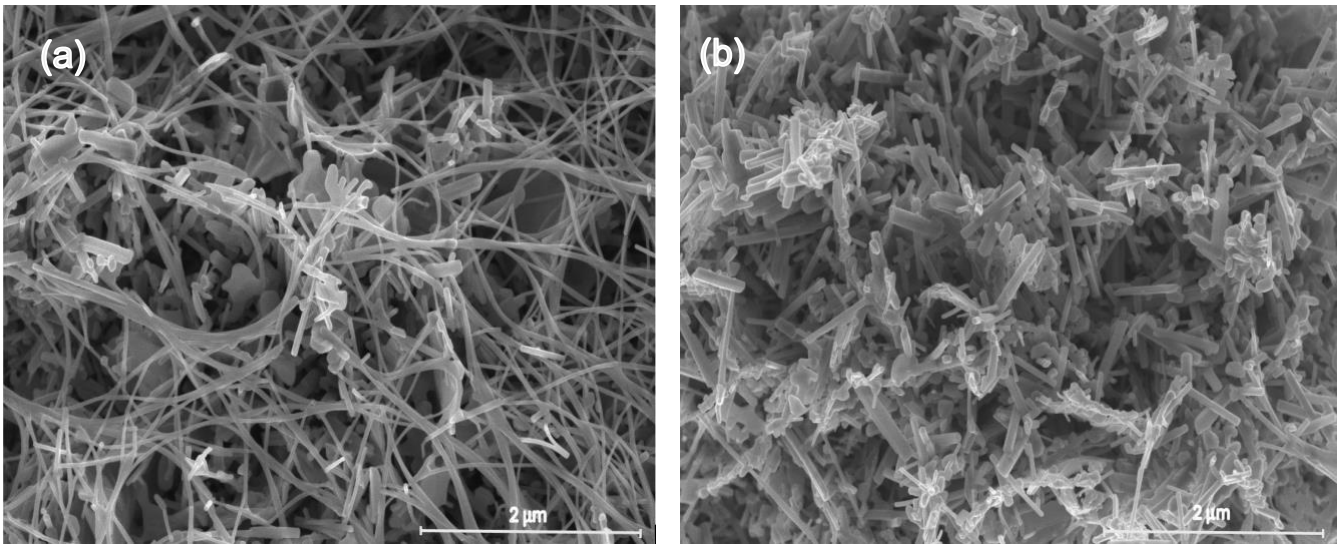

Figure 3-1: FESEM images of (a) pristine sodium hexa-titanates, (b) Ru-modified sodium hexa-titanates.

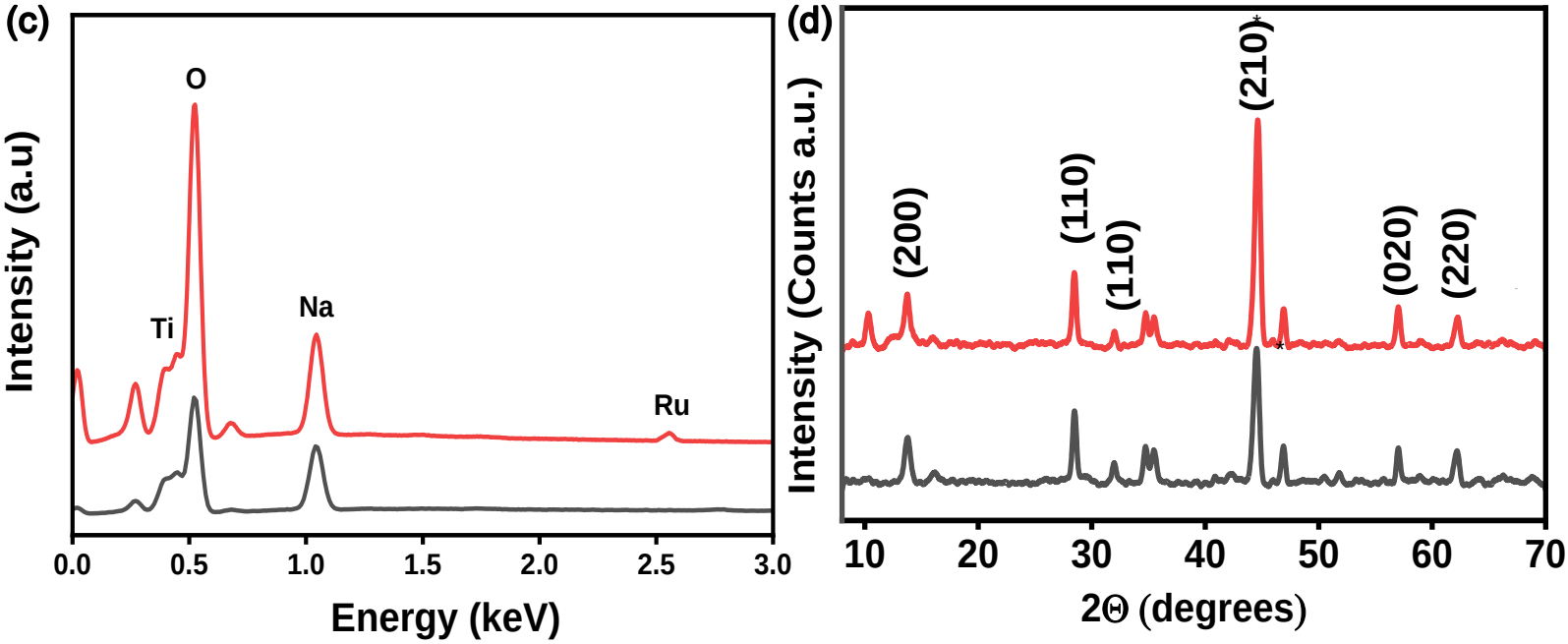

Figure 3-2: EDS spectra, (d) XRD spectra of pristine sodium hexa-titanates and Ru-modified sodium hexa-titanates

The EDS spectra in *Figure 3-2(a)* illustrate the material's elemental composition before and after the modification Ti/$Na_2Ti_6O_{13}$ nanocomposites with Ru. The trace amounts of Ru (0.4 µg cm^{-2}) show a Ru Lα x-ray emission peak at 2.56 K eV in EDS spectra, however it was not discernible from background. Therefore, the loading amount of Ru is increased ten-fold (4 µg) for confirming the presence of Ru on Ti/$Na_2Ti_6O_{13}$ nanocomposites (*Figure 3-2(a)*).

The crystallinity of sodium hexa-titanates samples was analyzed by XRD measurements. *Figure 3-2(d)* shows the XRD analysis of Ti/$Na_2Ti_6O_{13}$ and Ru-Ti/$Na_2Ti_6O_{13}$ annealed at temperatures of 650°C. The 2θ XRD values are recoded from range of 10 to 70° using cobalt radiation (λavg= 1.79026 Å). The characterization of crystallographic analysis of material using the XRD revealed confirmed the Ti/$Na_2Ti_6O_{13}$ structural features. TiO_2 occurs in three primary crystalline phases:

anatase, rutile, and brookite, where rutile being recognized as the most thermodynamically stable phase. Based on literature review regarding the conversion of brookite to anatase TiO_2 at temperature exceeding 500 °C, to its rutile state temperature ranging from 600 °C to 1200 °C [7, 8]. Nevertheless, at temperature below 200 °C the TiO_2 appears in amorphous form. Therefore, in this study to explore the structure property relationship of the modified and unmodified $Ti/Na_2Ti_6O_{13}$ nanocomposites with trace amounts of Ru, the annealing process was done at 150 °C, 350°C and 650°C to analyze their capacitive characteristics across different phases.

The diffractions peaks in the XRD spectra indicates the formation of rutile/anatase phases of TiO_2 with presence of sodium hexa-titanates. The peaks located at 13.7° and 28.5° have been attributed to (200) and (110) planes of sodium hexa-titanates [9]. Peaks observed at 31.9° has been designated to the (110) plane of the rutile TiO_2 phase. Sodium hexa-titanates lattice have dopants like larger Na ion replacing smaller Ti ion creating local distortion in lattice structures [10]. The distortion can be transformed in phases can be crystallized through annealing process. Since, the studies have also shown that Na doping can lower the temperature at which the anatase to rutile phase transition occurs, leading to the formation of $Ti/Na_2Ti_6O_{13}$ nanocomposites with local rutile/anatase phases of TiO_2 interspersed [11]. The intensity of the peaks of nanowires confirms the high crystallinity of the nanocomposites structure. The crystalline size can be estimated through Scherrer equation

$$D = \frac{\kappa\lambda}{\beta \cos\theta} \qquad \textit{Equation. (3-4)}$$

β is the full width at half-maximum (FWHM) of diffraction peak, λ is the X-ray wavelength (nm) and θ is the diffraction angle [12]. The average crystalline size calculated using the Scherrer equation is 18.03 nm for $Ti/Na_2Ti_6O_{13}$ nanocomposites and 17.72 nm for Ru modified $Ti/Na_2Ti_6O_{13}$ nanocomposites, showing that the Ru modification does exert a slight structural

modification in Ti/$Na_2Ti_6O_{13}$ nanocomposites. Due to high annealed temperature of TiO_2 can cause the eliminate of grain boundary defects, therefore the crystallite size can be increased [13]. The annealed temperature can assist the control the ratio of phase formation anatase and rutile phases [14].

In this work, the study is hypothesized that a successful introduction of oxygen vacancies into the lattice structure of Ti/$Na_2Ti_6O_{13}$ and Ru-Ti/$Na_2Ti_6O_{13}$ nanocomposites using EC treatment via chronopotentiometry as detailed in the methodology section, could improve the intrinsic C_{sp} of the ECSC material. Since oxygen vacancies are known to increase electrochemical active sites and impart high surface conductivity by improving electron transfer rates. Therefore, XPS spectra were obtained for the titanium orbitals and those for the O1s to investigate the surface chemical composition.

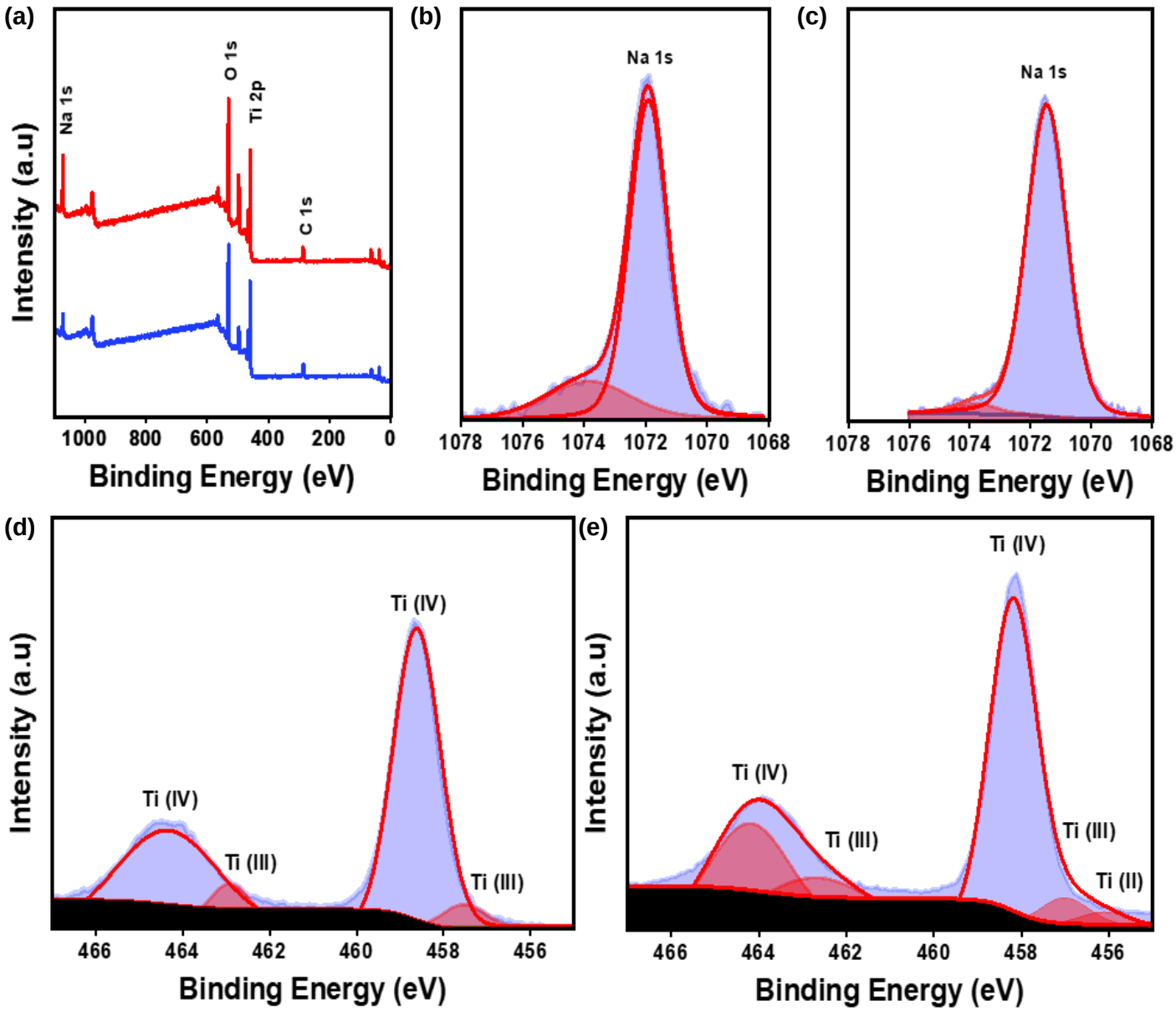

Figure 3-3: (a) XPS survey spectrum scans of Ti/$Na_2Ti_6O_{13}$ and Ru-Ti/$Na_2Ti_6O_{13}$ nanocomposites after EC treatment, (b) Na 1s peaks of Ti/$Na_2Ti_6O_{13}$ nanocomposites before EC treatment, (c) Na 1s peaks of Ti/$Na_2Ti_6O_{13}$ nanocomposites after EC treatment, (d) Ti 2p peaks of Ti/$Na_2Ti_6O_{13}$ nanocomposites before EC treatment and (e) Ti 2p peaks of Ti/$Na_2Ti_6O_{13}$ nanocomposites after EC treatment.

Figure 3-3(a) illustrates the survey spectrum, where the presence of Na, Ti, O signals are aligning with the elemental composition of Ti/$Na_2Ti_6O_{13}$ and Ru- Ti/$Na_2Ti_6O_{13}$ following their EC treatment. The minimal amount of Ru is practically detectable due to its ultra-low amounts of loading. *Figure 3-3(b)* displays Na 1s signal of Na^+ peaks at 1071.92 eV and 1073.84 eV before EC treatment and *Figure 3-3(c)* shows 1071.47 eV and 1073.7 eV after EC treatment of Ti/$Na_2Ti_6O_{13}$ nanocomposites. *Figure 3-3(d)* shows binding energies of Ti^{4+} and Ti^{3+} states were determined to be approximately 458.75 eV and 457.45 eV for Ti/$Na_2Ti_6O_{13}$ nanocomposites before EC treatment. *Figure 3-3(e)* shows binding energies of Ti^{4+}, Ti^{3+}, and Ti^{2+} states that were determined to be approximately 458.2, 457.15, and 456.0 eV respectively. These binding energies correspond to Ti (IV)-O, Ti (III)-O and Ti (II)-O bonds in the TiO_2 rutile phase [15]. Following the EC treatment, it was distinctly observable that was a reduction in atomic percentage of Ti (IV), and alongside a concurrent increase in atomic percentages of Ti (III) and Ti (II), respectively. After the EC treatment, these results indicate defects within the Ti/$Na_2Ti_6O_{13}$ nanocomposites.

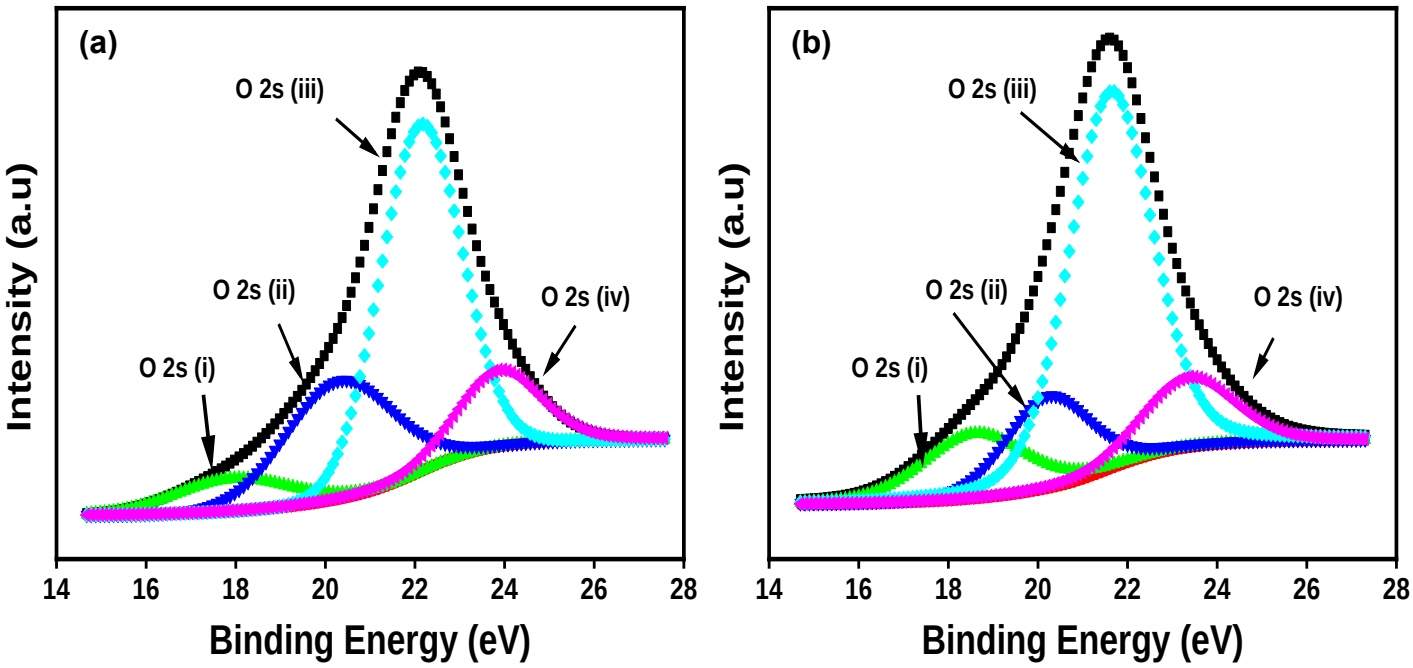

Figure 3-4: (a) O 2s individual atomic XPS spectra of (a) Ti/$Na_2Ti_6O_{13}$ before EC treatment (b) Ti/$Na_2Ti_6O_{13}$ after EC treatment

Figure 3-4 (a), show the deconvoluted individual plots of O 2s pertaining to Ti/$Na_2Ti_6O_{13}$. Due to Na KLL and O1s peaks overlap, therefore, O2s peaks were taken into consideration. O2s peaks in TiO_2 represent the lattice oxygen in crystal structure Four major peaks at 17.95, 20.32, 22.12 and 23.87 eV attributed to phase transformation of anatase, rutile or brookite as well as presence of lattice defects were observed in Ti/$Na_2Ti_6O_{13}$ [16]. Due to changes in peaks of O2s signal indicates the presence of oxygen vacancies. It reveals that the surface species do not change on modified electrodes due to the EC treatment process. We have identified that upon the EC treatment of Ti/$Na_2Ti_6O_{13}$ nanocomposites showed an improved C_{sp} values. This trend was also true in case of Ru-Ti/$Na_2Ti_6O_{13}$ nanocomposites. These trends of improved C_{sp} values via EC treatment and Ru modification of Ti/$Na_2Ti_6O_{13}$ nanocomposites will be discussed in the later sections of this study.

3.3.2. Electrochemical Characterization of $Na_2Ti_6O_{13}$ and Ru-$Na_2Ti_6O_{13}$

Electrochemical characterization of the electrodes with Ti/$Na_2Ti_6O_{13}$ and Ru-Ti/$Na_2Ti_6O_{13}$ nanocomposites were carried out using cyclic voltammetry (CV) technique at incremental scan rates from 10 mV s^{-1} to 40 mV s^{-1} in 0.1 M H_2SO_4 electrolyte at room temperature. The CVs curves were obtained and compared for Ti/$Na_2Ti_6O_{13}$ and Ru-Ti/$Na_2Ti_6O_{13}$ nanocomposites annealed at 150, 350 and 650 °C. These CV curves were also compared with before and after EC treatment of Ti/$Na_2Ti_6O_{13}$ and Ru-Ti/$Na_2Ti_6O_{13}$ nanocomposite electrodes that were cured at all three temperatures. *Figure 3-5 (a)* and *3-5 (b)*, shows CV curves pertaining to before and after EC treatment of Ti/$Na_2Ti_6O_{13}$ nanocomposite electrodes that were cured at 150°C. The CVs curves that occur have unstable curves at scan rate from 30 mV/s to 40 mV/s with low current density. *Figure 3-5 (c) - 3-5 (d)*, and *Figure 3-5 (e) - 3-5 (f)*, shows CV curves pertaining to before and after EC treatment of Ti/$Na_2Ti_6O_{13}$ cured at 350°C and 650°C respectively. The potential window of CV curves was set from 0.3 V to 0.9 V in a discernible non-faradaic region. With reference *to Eq 1*, the capacitance values obtained for Ti/$Na_2Ti_6O_{13}$ nanocomposite electrodes are 0.915 F cm^{-2}, 1.407 F cm^{-2} and 10.658 F cm^{-2} at a scan rate of 10mV/s for annealing temperatures of 150 °C, 350 °C and 650 °C, respectively. It is important to note that the calculated C_{sp} per gram of Ru loading is adopted as a comparative metric. However, there is zero amount (0 g) of Ru on the unmodified Ti/$Na_2Ti_6O_{13}$ nanocomposite electrodes, therefore in case of unmodified Ti/$Na_2Ti_6O_{13}$ nanocomposites we shall henceforth represent their capacitance per zero gram of Ru. In contrast, the calculated capacitance values after the EC treatment of Ti/$Na_2Ti_6O_{13}$ nanocomposite electrodes were found to be 0.991 F cm^{-2} g^{-1}, 2.029 F cm^{-2} g^{-1} and 15.786 F cm^{-2} g^{-1} for (0 g of Ru) at scan rates of 10 mV s^{-1} for 150 °C, 350 °C and 650 °C, respectively. Here the increased electrochemical capacitance after EC treatment as obtained from CVs is comprised of double layer capacitance

(C_{dl}) and pseudocapacitance, which is also a direct indicator of an overall increase electrochemical active surface area (EASA) due to the introduction of oxygen vacancies.

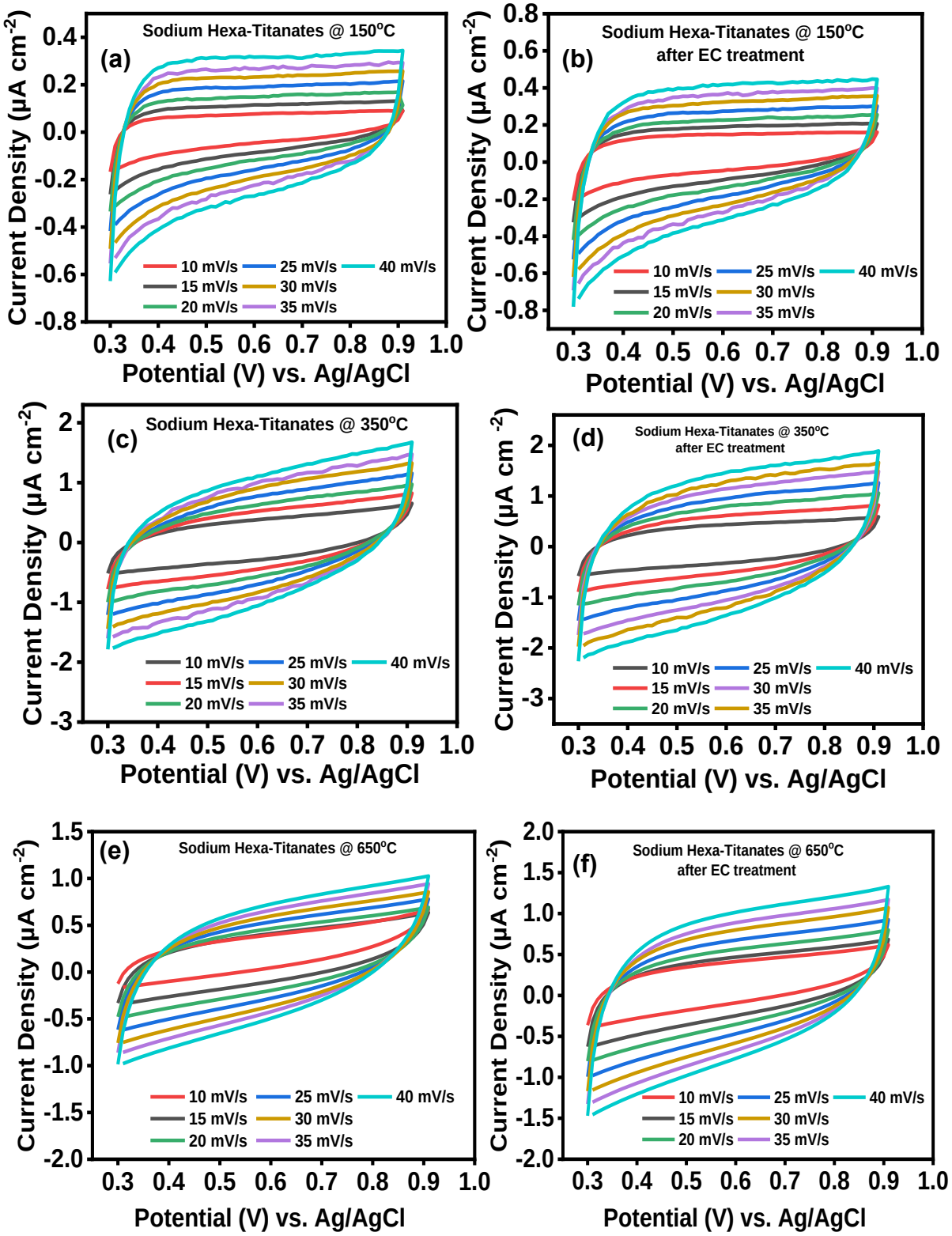

Figure 3-5: Cyclic voltammetry (CVs) curves for pristine sodium hexa-titanates were obtained from a scan rate of 10 to 40 mV s^{-1} (a-f) pristine sodium hexa-titanates annealed at 150°C, 350°C and 650°C before and after EC treatment step respectively.

For further enhancement of capacitance, the Ti/$Na_2Ti_6O_{13}$ nanocomposites were modified with trace amounts of Ru (0.4 µg) via drop-casting method. *Figure 3-6* shows the CV curves of Ru-Ti/$Na_2Ti_6O_{13}$ nanocomposite electrodes under identical conditions. The CVs curves of Ru-Ti/$Na_2Ti_6O_{13}$ show a partial rectangular shape, indicating the EDLC behaviour with redox peaks near potential 0.9 V representing the pseudocapacitance behaviour of Ru, thus demonstrating the higher synergistic effect of Ru-Ti/$Na_2Ti_6O_{13}$. The C_{sp} values of Ru-Ti/$Na_2Ti_6O_{13}$ were observed to be 22.35 F cm^{-2} g^{-1}, 70.72 F cm^{-2} g^{-1} and 272.34 F cm^{-2} g^{-1} at a scan rate of 10 mV/s for 150 °C, 350°C and 650°C, respectively. After EC treatment step, the C_{sp} was calculated as 28.35 F cm^{-2} g^{-1}, 80.95 F cm^{-2} g-1 and 325.88 F cm^{-2} g^{-1}, at a scan rate of 10 mV s^{-1} for 150, 350 and 650 °C, respectively, indicating the dramatic improvement in C_{sp} with introduction oxygen vacancies. *Figure 3-6 (a-f)*, shows plots of C_{sp} versus scan rates of electrodes before and after EC treatment that were cured at 150, 350 and 650 °C. There was a dramatic improvement of capacitance with annealing across all scan rates. The improvement in capacitance after EC treatment is more noticeable for electrodes that were annealed at 650 °C. This trend held true even for the Ru modified Ti/$Na_2Ti_6O_{13}$.

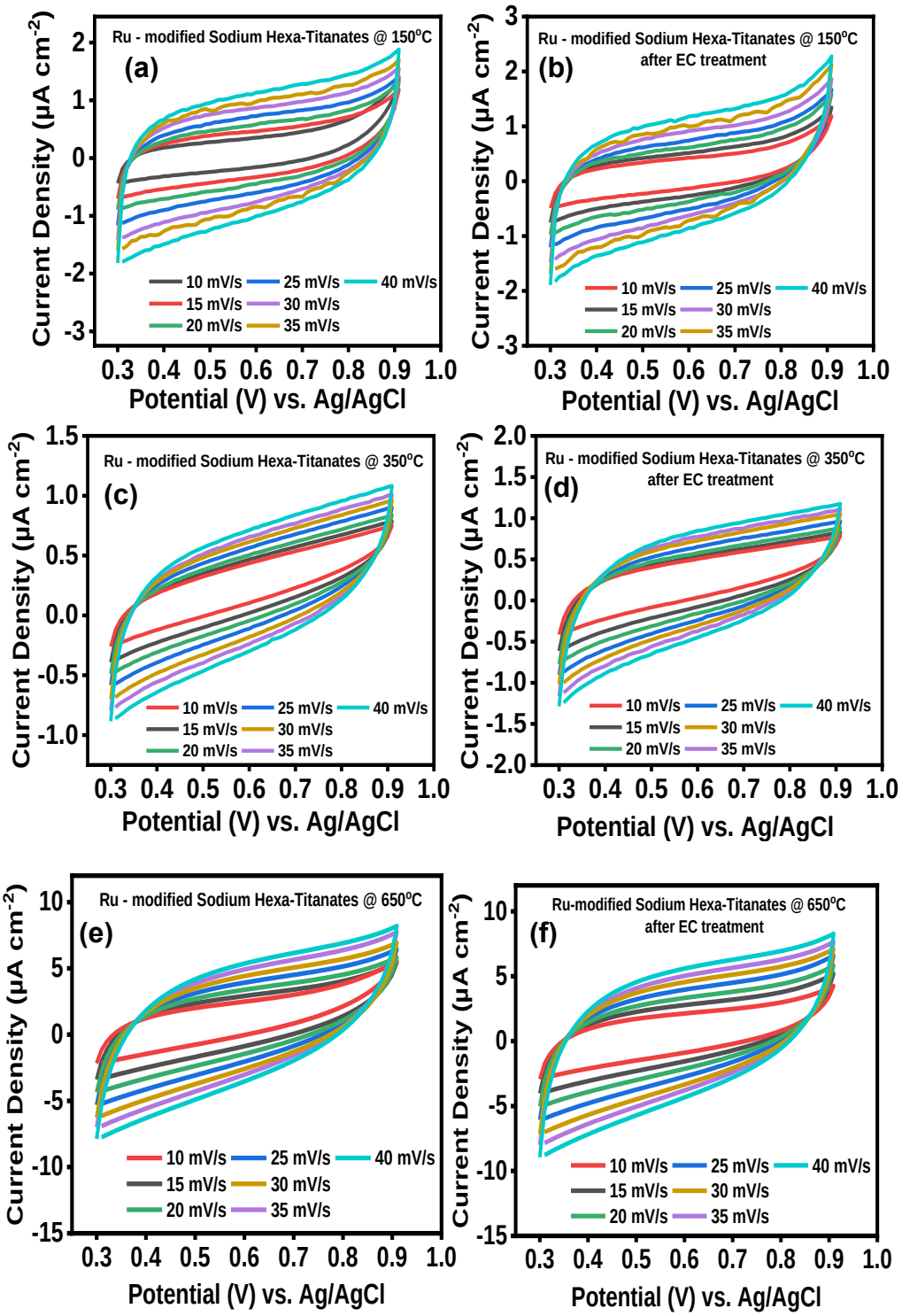

Figure 3-6: Cyclic voltammetry (CVs) curves for Ru modified sodium hexa-titanates were obtained from a scan rate of 10 to 40 mV s^{-1} (a-f) annealed at 150°C, 350°C and 650°C before and after EC treatment step respectively.

The specific capacitance of the samples decreases with the scan rate increases depicted in *Figure 3-7* can be attributed to a redox reaction on the electrode, which reduces the transportation of ions into the active material [17]. At higher scan rates electrolyte ions do not have sufficient time to penetrate deep into electrode pores. At slower scan rates, the ions can great contact with the internal surface of electrode, yields at higher capacitance values [18].

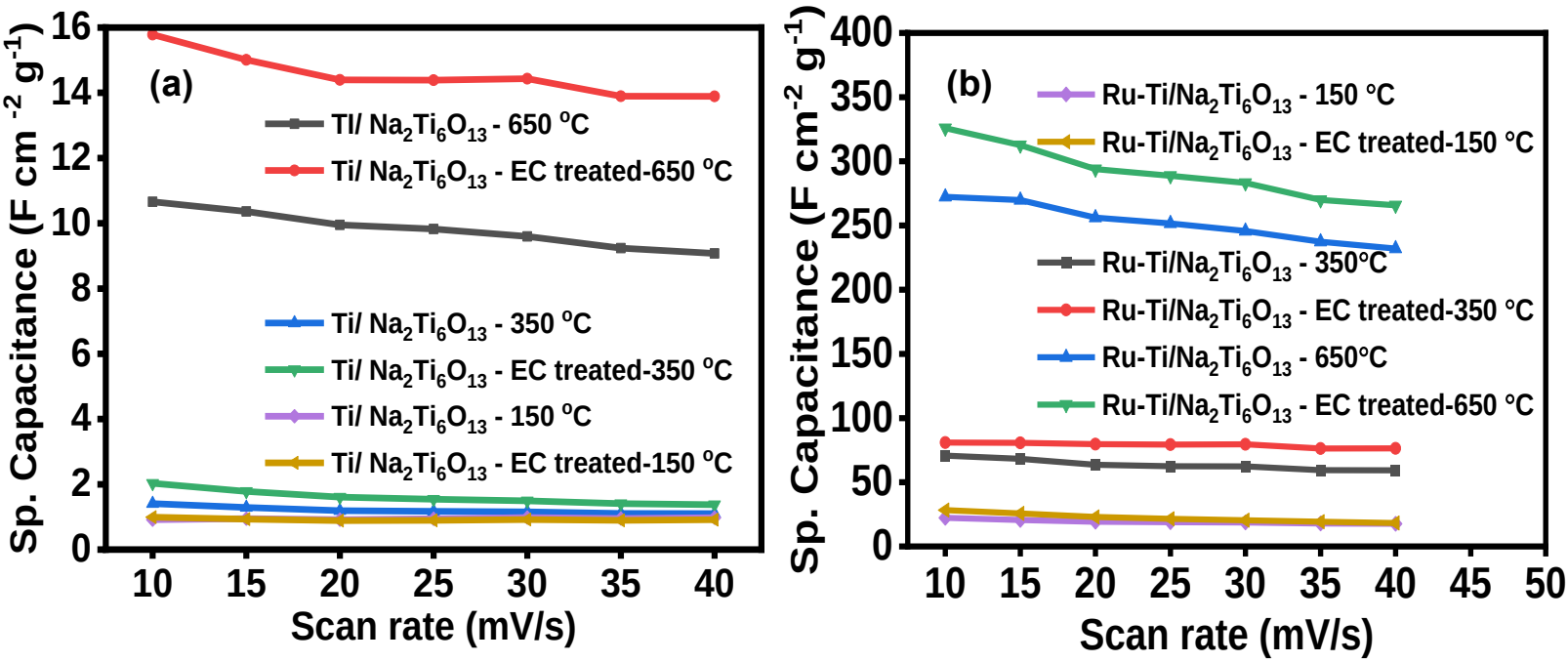

Figure 3-7: The specific capacitance of both (e) pristine sodium hexa–titanates and (f) Ru-modified sodium hexa-titanates measured as a function of scan rate.

Galvanostatic charge and discharge cycles (GCD), depicted in *Figure 3-8 and 3-9* have been conducted on both Ti/$Na_2Ti_6O_{13}$ and Ru-Ti/$Na_2Ti_6O_{13}$ in 0.1 M of H_2SO_4 electrolyte, measured at different current densities of 1, 2, 3, 10 µA within a constant potential window of 0-0.9 V vs. Ag/AgCl. GCD curves have exhibited suitable linear symmetry shapes over the current densities of 1, 2, 3, 10 µA, revealing a large contribution of fast and accessible C_{dl} to the overall capacitive behaviour. GCD cycles were performed for each annealing temperature, and at different rates of charging and discharging capabilities were explored. *Figure 3-8 (a)* illustrate the GCD curves of Ti/$Na_2Ti_6O_{13}$ at current density of 1 µA for each annealing temperature.

The discharging time increases consecutively from 150 to 650 °C. The C_{sp} values from the GCD plots were calculated from Eq 2. The highest specific capacitance was achieved at a current density of 1 µA for a 650 °C electrode, which was found to be 10.317 F cm^{-2} g^{-1}, illustrating the impact of temperature on electrochemical performance [19]. The electrodes were subjected to EC treatment to create oxygen vacancies and were later tested for GCD curves for each annealing temperature at the current density of 1 µA. It was observed that the discharge time further increases for each annealed temperature, causing slower transport of electrolyte ions. The calculated specific capacitance after EC treatment was 15.873 F $cm^{-2}g^{-1}$ at a current density of 1 µA for 650 °C electrode. We focused on the results for 650 °C annealing temperature due to the longest charge-discharge time. It is noted that charging/discharging time decreases at higher current density due to the fast diffusion of ions on the electrode surface, thereby affecting the charge storage capability [20-23]. This is illustrated in *Figure 3-8(c)* & *Figure 3-8(d)*, which shows GCD curves for 650 °C electrodes measured at various current densities of 1, 2, 3, 10 µA. The calculated C_{sp} for Ti/$Na_2Ti_6O_{13}$ were 8.7230, 6.904 and 1.112 F $cm^{-2}g^{-1}$ at 2, 3, 10 µA current densities before EC

treatment. Similarly, C_{sp} after EC treatment was found to be 11.904 F $cm^{-2}g^{-1}$, 7.936 F $cm^{-2}g^{-1}$, 1.468 F $cm^{-2}g^{-1}$ at 2, 3, 10 µA.

Figure 3-8(a-b) and *3-9(a-b)*, demonstrates that at lower annealing temperatures of 150°C and 350 °C, the EC treatment enhanced their capacitance as observed by longer charge-discharge times. However, for the sample annealed at 650 °C, the change is small before and after EC treatment. This can be explained by comparing the resistive (V=IR) and capacitive (V=Q/C) potential components. *Figure 3-8* & *3-9* shows that samples annealed at higher temperatures demonstrate higher IR drop. This is also evident by looking at the slope of the CV curves in *Figure 3-5(e-f) to 3-6(e-f)* compared to the slope (or lack thereof) of CV curves in *Figure 3-5(a-d) to 3-6(a-d)*. This is likely due to the formation of thicker layers of oxides at higher annealing temperatures. The value of the IR drop and its change before and after EC treatment is not significant at a lower current, which is 1 µA. However, the resistive contribution is much more apparent at higher currents in *Figure 3-5(e-f)*, where the sample before EC treatment is much more resistive than the reduced sample.

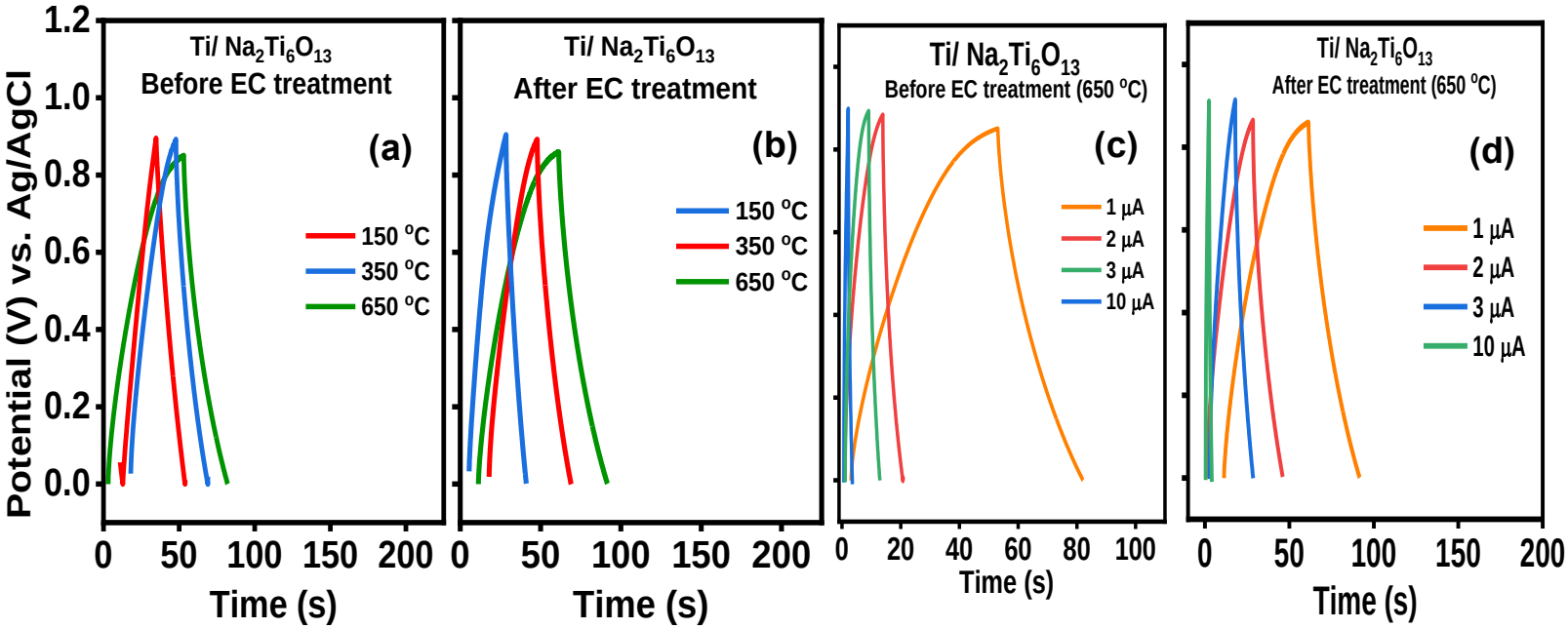

Figure 3-8: Galvanostatic charge-discharge curves (GCD) of (a) pristine sodium hexa – titanates at different annealing temperatures before treatment, (b) after treatment, (c)(d) GCD curves of 650°C collected at different current densities of 1 µA,2 µA,3 µA and 10 µA before and after EC treatment respectively.

Figure 3-9, present the GCD curves of modified electrodes with Ru-Ti/$Na_2Ti_6O_{13}$ at different annealing temperatures, shows an excellent symmetric shape with a linear slope. The specific capacitance of 650 °C with modification of Ru was calculated through Eq 2 was 31.423 F $cm^{-2}g^{-1}$ and 64.320 F $cm^{-2}g^{-1}$ before and after EC treatment The GCD curves were obtained at 1, 2, 3, 10 µA current densities and exhibited good cycling behaviour. *Figure 3-9 (c) and 3-9 (d)*, shows a 650 °C electrode with modification of Ru at 1, 2, 3, 10 µA current densities with calculated capacitance of 30.904, F $cm^{-2}g^{-1}$, 18.730 F $cm^{-2}g^{-1}$, 1.587 F $cm^{-2}g^{-1}$ and 63.285 F $cm^{-2}g^{-1}$, 60.317 F $cm^{-2}g^{-1}$, 1.984 F $cm^{-2}g^{-1}$ before and after EC treatment, respectively. These samples exhibit the longest charge-discharge time, indicating good specific capacitive performance.

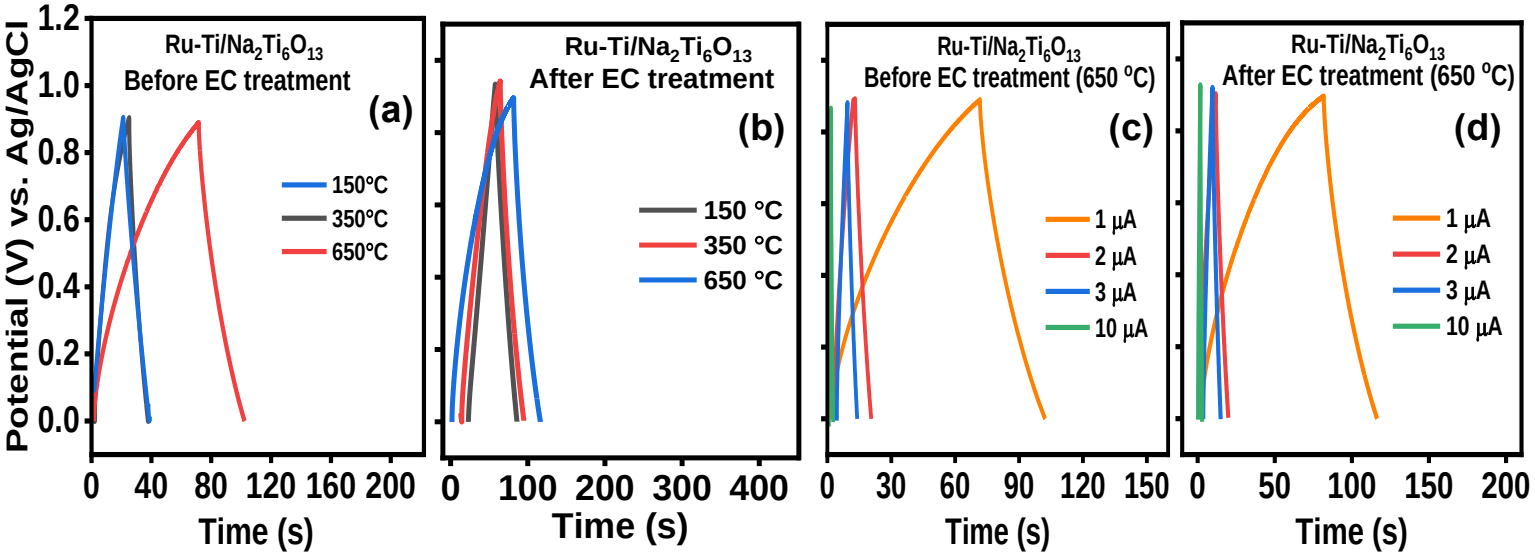

Figure 3-9: Galvanostatic charge-discharge curves (GCD) of (a) Ru modified sodium hexa – titanates at different annealing temperatures before treatment, (b) after treatment, (c)(d) GCD curves of 650°C collected at different current densities of 1 µA,2 µA,3 µA and 10 µA before and after EC treatment respectively.

The GCD measurements were obtained 2000 cycles to get additional information on the cycling behaviour and stability of the electrode at 1 µA current density. *Figure 3-10* demonstrate the calculated capacitance retention of the electrodes annealed at 650 °C after 2000 cycles at about 81% and 83% at 1 µA for samples without and with EC treatment, respectively. Furthermore, the GCD curves of 650 °C remained unchanged, showing a symmetric and linear triangular shape after 2000 cycles both before and after introducing oxygen vacancies by EC treatment. The stability of oxygen vacancies on lattice structure were demonstrated by the stable cycling of electrodes after 2000 cycles. Further, cycling stability tests were carried out for a 650 °C electrode with Ru for 2000 cycles at a current density of 1 µA. The retention after 2000 cycles were found to be 86% and 87% at 1 µA, before and after EC treatment respectively.

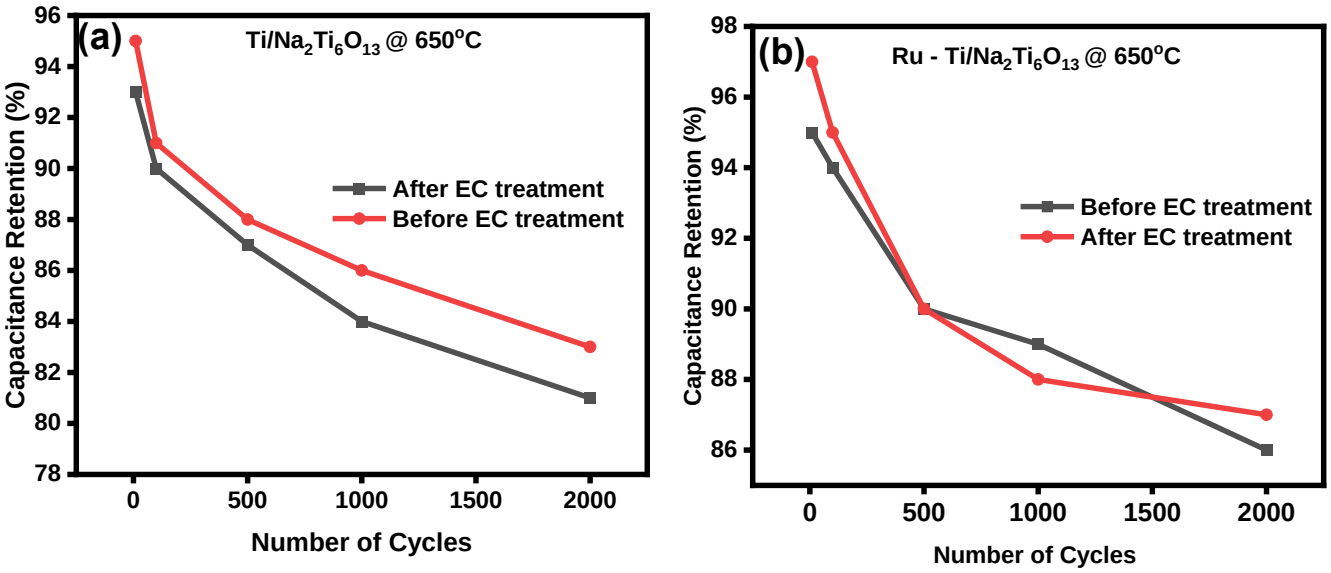

Figure 3-10: Cycling stability of (a) pristine sodium hexa – titanates (b) Ru modified sodium hexa – titanates

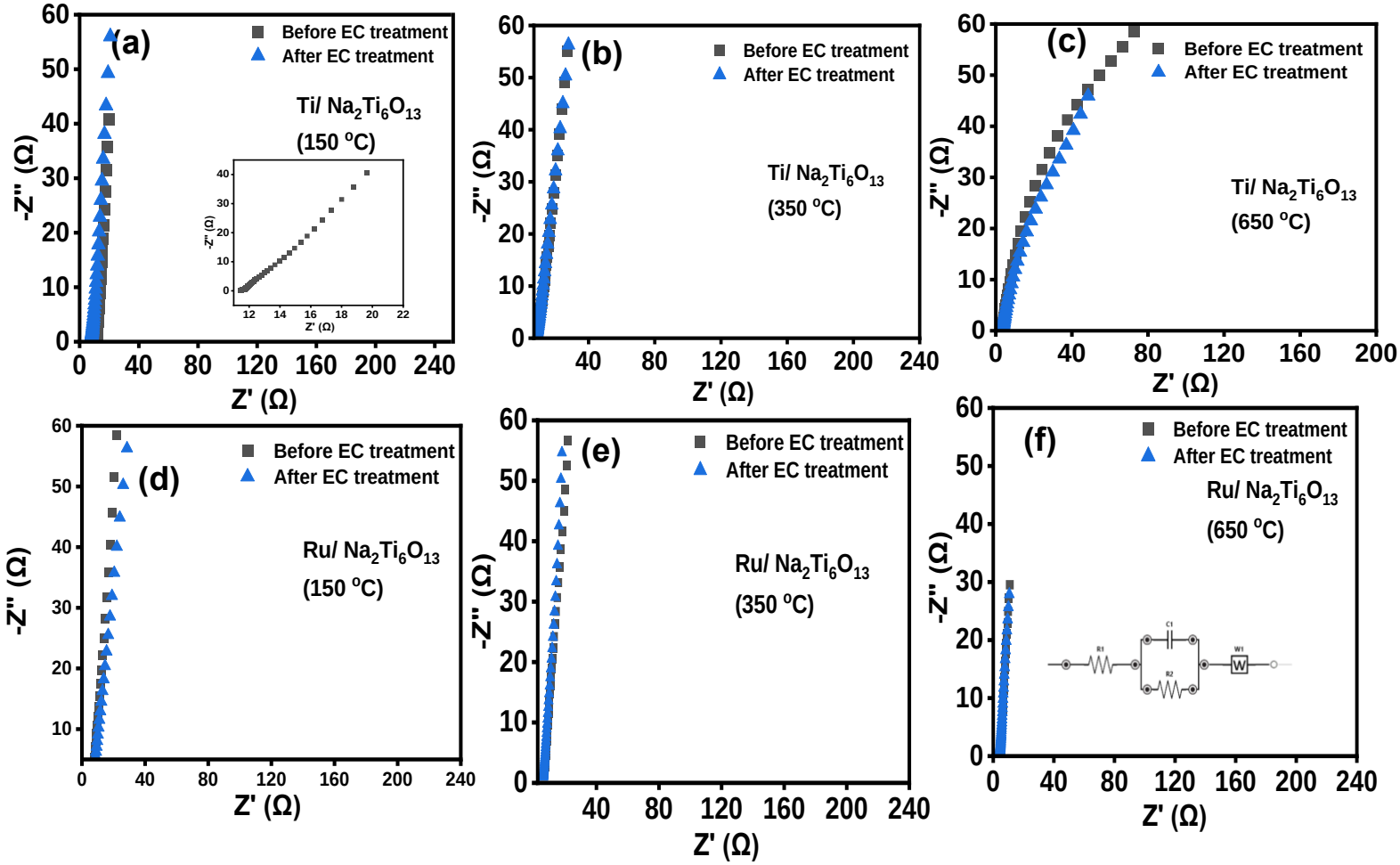

Figure 3-11: Nyquist plots of pristine sodium hexa-titanates and Ru modified of sodium hexa-titanates with inset of the equivalent circuit diagram at annealed temperatures of 150°C, 350°C and 650 °C before and after treatment collected at frequencies from 100,000 Hz to 100 Hz.

Electrochemical impedance tests (EIS) were performed on Ti/$Na_2Ti_6O_{13}$ and Ru-Ti/$Na_2Ti_6O_{13}$ nanocomposite electrodes to determine the electrical conductivity and charge transfer resistance. *Figure 3-11* represents Nyquist plots of Ti/$Na_2Ti_6O_{13}$ nanocomposite electrodes before and after EC treatment of all annealing temperatures. The tests were conducted in 0.1 M of H_2SO_4 with a frequency range of 100,000 to 100 Hz and E_{DC} at 0.6 V. The Ti/$Na_2Ti_6O_{13}$ nanocomposite electrode before EC treatment has shown higher impedance values. To assess the charge transfer properties on electrode surface, the Nyquist plots were fitted with the creation of an equivalent circuit diagram (*Figure 3-11(f)* inset). In this inset, R1 represents the electrolyte resistance, R2 represents the charge transfer between the electrode surface and electrode, C1 represents the capacitive nature, and W1 represents the Warburg diffusion coefficient. The impedance intercept in the high frequency range on real axis represent the equivalent series resistance (ESR) of the system. Usually, the formation of semicircles on Nyquist plots shows the electrode resistance and the material's conductivity [24]. The formation of arc in the low-frequency range represents the beginning of charge-transfer reaction. Due to the introduction of oxygen vacancies, the resistance values decrease, contributing to an enhanced electrical conductivity. The 650 °C electrodes indicate a steeper slope in the low-frequency region, indicating good capacitive behaviour. Impedance tests were conducted on Ru-Ti/$Na_2Ti_6O_{13}$ nanocomposite electrodes, which was demonstrated in *Figure 3-11 (d-f)* at all annealing temperatures with similar conditions. Ru-modified sodium hexa-titanates 650 °C electrodes observed no semicircle at the higher frequency range. The straight line corresponds to the Warburg diffusion coefficient due to ionic diffusion. Furthermore, an EIS analysis of Ru-Ti/$Na_2Ti_6O_{13}$ versus Ti/$Na_2Ti_6O_{13}$ as presented *Table 3-1* the calculated values of circuit diagram, reveals the reduction in uncompensated film resistance (R1)

and charge transfer resistance (R2) with Ru modification accompanied with significantly higher capacitance. This signifies an improvement in resistance and capacitance of the nanocomposite material with introduction of ultra-low amounts of ruthenium.

Table 3-1: Calculated values of an equivalent circuit diagram for samples before EC treatment and after EC treatment, respectively

Samples	**Annealed Temperature (°C)**	**R1 (Ohms)**	**R2 (Ohms)**	**C1 (F)**	**W1**
sodium hexa-titanates	150	11.21	312.5	16.43	0.131
	350	7.796	222.0	30.71	0.336
	650	2.812	87.05	44.29	0.503
Ru modified sodium hexa-titanates	150	4.485	170.3	19.33	0.071
	350	5.417	140.8	47.70	0.354
	650	2.552	69.9	143.11	3.520
Samples	**Annealed Temperature (°C)**	**R1 (Ohms)**	**R2 (Ohms)**	**C1 (F)**	**W1**
sodium hexa-titanates	150	7.295	295.4	24.29	0.202
	350	7.453	200.7	39.29	0.544
	650	1.778	56.91	51.43	1.508
Ru modified sodium hexa-titanates	150	4.243	130.1	37.66	0.060
	350	5.371	100.5	80.34	0.194
	650	2.113	39.5	148.13	3.895

3.4. Conclusion

In this chapter, a facile two-step process has been developed to synthesize or grow $Na_2Ti_6O_{13}$ nanocomposites on a Ti metal substrate surface using a hydrothermal process and later annealed at different temperatures for phase transformation. Subsequently, oxygen vacancies were successfully introduced into the lattice structure of the $Na_2Ti_6O_{13}$ nanocomposites, which showed an observable enhancement in its specific capacitance (C_{sp}). The electrical conductivity and charge transfer significantly improved after introducing oxygen vacancies via EC treatment methodology. The CV curves indicated that the C_{sp} of electrodes increases as annealing temperatures increase. The C_{sp} reported for $Na_2Ti_6O_{13}$ nanocomposites was 10.658 F cm^{-2} g^{-1} before EC treatment and 15.786 F cm^{-2} g^{-1} after EC treatment at a scan rate of 10 mV s^{-1} with excellent charge-discharge rate capability. Further, to enhance the C_{sp}, trace amounts of Ru was deposited on the surface of the Ti/$Na_2Ti_6O_{13}$ nanocomposites coupled with oxygen reduction procedure, which led to a dramatic increase in C_{sp}. The highest C_{sp} achieved with Ru modification was 272.34 F cm^{-2} g^{-1} before inducing oxygen vacancies and was further enhanced to 325.88 F cm^{-2} g^{-1} with introduction of oxygen vacancies. Our experiments demonstrate that the modified sodium hexa-titanates with trace amounts of ruthenium can be used as an electrode material for high-performance supercapacitor applications in future.

3.5. References

[1] B. Evanko, S. W. Boettcher, S. J. Yoo, and G. D. Stucky, "Redox-Enhanced Electrochemical Capacitors: Status, Opportunity, and Best Practices for Performance Evaluation," *ACS Energy Lett.*, vol. 2, no. 11, pp. 2581–2590, Nov. 2017, doi: 10.1021/acsenergylett.7b00828.

[2] L. Kouchachvili, W. Yaïci, and E. Entchev, "Hybrid battery/supercapacitor energy storage system for the electric vehicles," *Journal of Power Sources*, vol. 374, pp. 237–248, Jan. 2018, doi: 10.1016/j.jpowsour.2017.11.040.

[3] B. K. Kim, S. Sy, A. Yu, and J. Zhang, "Electrochemical Supercapacitors for Energy Storage and Conversion," in *Handbook of Clean Energy Systems*, John Wiley & Sons, Ltd, 2015, pp. 1–25. doi: 10.1002/9781118991978.hces112.

[4] S. Sharma and P. Chand, "Supercapacitor and electrochemical techniques: A brief review," *Results in Chemistry*, vol. 5, p. 100885, Jan. 2023, doi: 10.1016/j.rechem.2023.100885.

[5] M. Sethi, U. S. Shenoy, and D. K. Bhat, "A porous graphene–NiFe2O4 nanocomposite with high electrochemical performance and high cycling stability for energy storage applications," *Nanoscale Adv.*, vol. 2, no. 9, pp. 4229–4241, Sep. 2020, doi: 10.1039/D0NA00440E.

[6] V. C. Anitha, A. N. Banerjee, G. R. Dillip, S. W. Joo, and B. K. Min, "Nonstoichiometry-Induced Enhancement of Electrochemical Capacitance in Anodic TiO2 Nanotubes with Controlled Pore Diameter," *J. Phys. Chem. C*, vol. 120, no. 18, pp. 9569–9580, May 2016, doi: 10.1021/acs.jpcc.6b01171.

[7] M. Amiri, J. Dondapati, J. Quintal, and A. Chen, "Sodium Hexa-Titanate Nanowires Modified with Cobalt Hydroxide Quantum Dots as an Efficient and Cost-Effective Electrocatalyst for Hydrogen Evolution in Alkaline Media," *ACS Appl. Mater. Interfaces*, vol. 14, no. 35, pp. 40021–40030, Sep. 2022, doi: 10.1021/acsami.2c11310.

[8] S. Arshadi Rastabi, R. Sarraf-Mamoory, G. Razaz, N. Blomquist, M. Hummelgård, and H. Olin, "Treatment of NiMoO4/nanographite nanocomposite electrodes using flexible graphite substrate for aqueous hybrid supercapacitors," *PLoS One*, vol. 16, no. 7, p. e0254023, 2021, doi: 10.1371/journal.pone.0254023.

[9] R. S. Dubey, "Temperature-dependent phase transformation of TiO2 nanoparticles synthesized by sol-gel method," *Materials Letters*, vol. 215, pp. 312–317, Mar. 2018, doi: 10.1016/j.matlet.2017.12.120.

[10] M. M. El-Desoky, I. Morad, M. H. Wasfy, and A. F. Mansour, "Synthesis, structural and electrical properties of PVA/TiO2 nanocomposite films with different TiO2 phases prepared by sol–gel technique," *J Mater Sci: Mater Electron*, vol. 31, no. 20, pp. 17574–17584, Oct. 2020, doi: 10.1007/s10854-020-04313-7.

[11] P. Prasannalakshmi, N. Shanmugam, A. S. kumar, and N. Kannadasan, "Phase-dependent electrochemistry of TiO2 nanocrystals for supercapacitor applications," *Journal of Electroanalytical Chemistry*, vol. 775, pp. 356–363, Aug. 2016, doi: 10.1016/j.jelechem.2016.06.027.

[12] U. Diebold and T. E. Madey, "TiO2 by XPS," *Surface Science Spectra*, vol. 4, no. 3, pp. 227–231, Jul. 1996, doi: 10.1116/1.1247794.

[13] Y. Zhang, X. Li, Z. Li, and F. Yang, "Evaluation of electrochemical performance of supercapacitors from equivalent circuits through cyclic voltammetry and galvanostatic charge/discharge," *Journal of Energy Storage*, vol. 86, p. 111122, May 2024, doi: 10.1016/j.est.2024.111122.

[14] "IR drop studies of poly(aniline)-based modified electrodes - ScienceDirect." Accessed: Nov. 30, 2024. [Online]. Available: https://www.sciencedirect.com/science/article/pii/S1572665720308900

[15] S. Alkhalaf *et al.*, "Electrochemical energy storage performance of electrospun CoMn2O4 nanofibers," *Journal of Alloys and Compounds*, vol. 692, pp. 59–66, Jan. 2017, doi: 10.1016/j.jallcom.2016.09.005.

[16] D. Ghosh, S. Giri, and C. K. Das, "Synthesis, characterization and electrochemical performance of graphene decorated with 1D NiMoO4·nH2O nanorods," *Nanoscale*, vol. 5, no. 21, pp. 10428–10437, Oct. 2013, doi: 10.1039/C3NR02444J.

[17] X. Xu, J. Shen, N. Li, and M. Ye, "Microwave-assisted synthesis of graphene/CoMoO4 nanocomposites with enhanced supercapacitor performance," *Journal of Alloys and Compounds*, vol. 616, pp. 58–65, Dec. 2014, doi: 10.1016/j.jallcom.2014.07.047.

[18] L. Zhu *et al.*, "Pseudocapacitive Behavior of Ce Modified CoO through a Galvanostatic Charge–Discharge Test: Distinguishing between Surface-Control and Diffusion-Control Current," *J. Phys. Chem. C*, vol. 126, no. 25, pp. 10327–10334, Jun. 2022, doi: 10.1021/acs.jpcc.2c02518.

[19] A. Sarkar, A. K. Singh, D. Sarkar, G. G. Khan, and K. Mandal, "Three-Dimensional Nanoarchitecture of BiFeO $_3$ Anchored TiO $_2$ Nanotube Arrays for Electrochemical Energy Storage and Solar Energy Conversion," *ACS Sustainable Chem. Eng.*, vol. 3, no. 9, pp. 2254–2263, Sep. 2015, doi: 10.1021/acssuschemeng.5b00519.

[20] J. Zhang *et al.*, "Remarkable supercapacitive performance of TiO2 nanotube arrays by introduction of oxygen vacancies," *Chemical Engineering Journal*, vol. 313, pp. 1071–1081, Apr. 2017, doi: 10.1016/j.cej.2016.11.004.

[21] R. Reece, C. Lekakou, and P. A. Smith, "A High-Performance Structural Supercapacitor," *ACS Appl. Mater. Interfaces*, vol. 12, no. 23, pp. 25683–25692, Jun. 2020, doi: 10.1021/acsami.9b23427.

[22] A. Thejas Prasannakumar, R. R., J. Cherusseri, R. R.Mohan, and S. J. Varma, "High areal capacitance and long cycling stability in asymmetric supercapacitors using binder-free, hierarchical nanostructured Ni3S2/MnO2 hybrid electrodes," *Journal of Energy Storage*, vol. 55, p. 105723, Nov. 2022, doi: 10.1016/j.est.2022.105723.

[23] B. Choudhury and A. Choudhury, "Local structure modification and phase transformation of TiO2 nanoparticles initiated by oxygen defects, grain size, and annealing temperature," *Int Nano Lett*, vol. 3, no. 1, p. 55, Nov. 2013, doi: 10.1186/2228-5326-3-55.

[24] M. Y. Perdana *et al.*, "Understanding the Behavior of Supercapacitor Materials via Electrochemical Impedance Spectroscopy: A Review," *The Chemical Record*, vol. 24, no. 5, p. e202400007, 2024, doi: 10.1002/tcr.202400007.

Chapter 4: Sodium Hexa-titanate and Cobalt oxides hybrid-based nanocomposites to further enhance the supercapacitance

4.1. Introduction

Technological revolution have resulted in higher carbon dioxide emissions and fossil fuel consumption, which have driven global climate change. Thus, the depletion of fossil fuel resources and environmental problems cause a focus on energy storage distribution [1,2]. Among many TMOs, cobalt oxide (Co_3O_4) exhibits high theoretical specific capacitance due to its excellent capacitive performance, environmental capability, thermal stability, corrosion stability and pseudocapacitive behaviour [3,4]. Cobalt's natural abundance can make them more economically feasible than other TMO electroactive materials such as RuO_2. In general, TMOs possess challenges in terms of resistivity in high-performance SCs. This can be improved by introducing vacancies through doping or sintering [5]. It has been established that recently mixing one metal oxide with another oxide can give a synergistic effect, which in turn affects the facilitation of electrode/electrolyte charge diffusion, thus improving storage performance [6,7].

Sodium and potassium titanates have been implemented for sodium-ion batteries' anode applications. There is no research on sodium titanate nanowires or hybrid-based titanates for supercapacitor applications. . In the work relating to this chapter, a facile process has been developed to grow $Na_2Ti_6O_{13}$ nanocomposites on a Ti metal substrate surface using a hydrothermal method. Further, to enhance the Csp, Co_3O_4 nanoparticles were drop-casted on the surface of the Ti / $Na_2Ti_6O_{13}$ nanocomposites coupled with an oxygen reduction procedure to introduce oxygen vacancies into the lattice structure of the Co_3O_4 – $Na_2Ti_6O_{13}$nanocomposites which led to the improved Csp.

4.2. Experimental Details

4.2.1. Materials and Solutions:

Highly pure (99%) Titanium (Ti) plate foil (Grade 2) were purchased from McMaster-Carr. Chemicals like sodium hydroxide (NaOH), sulfuric acid (H_2SO_4), Cobalt (II) Chloride and 18% hydrochloric acid (HCl) were purchased from Sigma Aldrich. The electrochemical cell, Ag/AgCl reference electrode and platinum wire counter electrodes were purchased from BASi research products. All the electrochemical experiments were conducted using the PalmSens4 potentiostat.

4.2.2. Preparation of $Na_2Ti_6O_{13}$ and Co_3O_4-$Na_2Ti_6O_{13}$

A hydrothermal method was employed to synthesize the $Na_2Ti_6O_{13}$ nanowires and nanoplate structures (henceforth called nanocomposites) on the surface of a Ti metal plate. First, Ti plates of 1 cm^2 area and a thickness of 0.25 mm were cut from a larger metal plate. These Ti plates or electrodes were cleaned by sonification in acetone and deionized water for about 5 minutes. Then, they were etched with the boiling HCL (18%) for 15 mins. The etched electrodes were stored in deionized water for further use. The etched electrodes were put in a Teflon-lined autoclave vessel (of 100 mL capacity) containing 40 mL of 1 M NaOH to carry out a hydrothermal process at 200°C for 24 hrs [8]. After the hydrothermal treatment, the electrodes were washed several times with ultrapure water and were subsequently annealed at 150°C, 350°C and 650°C, respectively, for 3 h using a muffle furnace (Gilson company model: MF-2A) to obtain $Na_2Ti_6O_{13}$ nanocomposites with the capacitive performance. Subsequently, a 1 M NaOH solution was added dropwise into a mixture containing $CoCl_2 \cdot 6H_2O$ dissolved in 20 mL of deionized water over the course of approximately 5 minutes. The resulting mixture was then sonicated for an additional 60 minutes. Finally, mixture was transferred into a Teflon reactor with a stainless-steel coating to conduct a hydrothermal process at 180°C for 8 hrs [9]. All characterization and electrochemical techniques followed are similar to the one described in Chapter 3.3.2 and 3.3.3.

4.3. Results and Discussion

4.3.1 Characterization of Co_3O_4 - $Na_2Ti_6O_{13}$

Sodium Hexa-Titanates ($Na_2Ti_6O_{13}$) nanowires and nanoplate structures were synthesized on a Ti plate and Cobalt oxide (Co_3O_4) nanoparticles through hydrothermal method on surface of Ti plate. The morphology of this hybrid nanocomposites was investigated through an environmental scanning electron microscope (ESEM). *Figure 4-1 (a)* shows the composition of Co_3O_4 - Ti/$Na_2Ti_6O_{13}$ hybrid nanocomposites. It confirms the illustration of thin and long nanowire structures and spherical cobalt oxide structures uniformly spread on the Ti surface with an average of 0.1462 µm and 0.1896 µm, respectively.

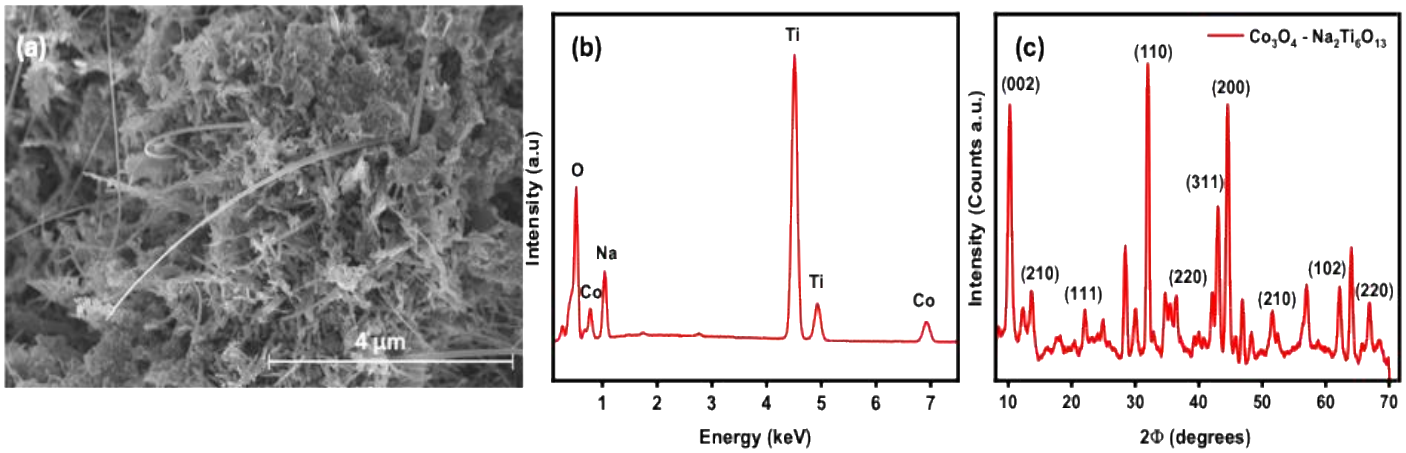

Figure 4-1: FESEM images of (a) Co_3O_4 - Ti/$Na_2Ti_6O_{13}$, (b) EDS spectra, (c) XRD spectra of Co_3O_4 - Ti/$Na_2Ti_6O_{13}$

The EDS spectra in *Figure 4-1(b)* illustrate the material's elemental composition with modification of Co_3O_4 - Ti/$Na_2Ti_6O_{13}$ hybrid nanocomposites. Co_3O_4 nanoparticles (0.5 µg cm^{-2}) shows a Co Lα and Kα x-ray emission peak at 0.7 K eV and 6.9 K eV respectively in EDS spectra. However,

loading amount of Co_3O_4 nanoparticles increases ten-fold (5 µg) for confirming the presents of Co_3O_4 nanoparticles Ti/$Na_2Ti_6O_{13}$.

Furthermore, *Figure 4-1(c)* shows the XRD analysis of Co_3O_4 - Ti/$Na_2Ti_6O_{13}$ hybrid nanocomposites annealed at 650 °C. The characterization of crystallographic analysis of material using the XRD revealed confirmed the Co_3O_4 - Ti/$Na_2Ti_6O_{13}$ structural features. As TiO_2 exists in three main crystalline phases, rutile being the most thermodynamically stable phase. It is well founded in literature about the transformation of brookite to anatase TiO_2 above 500 °C [10]. However, below 200 °C the TiO_2 exists in amorphous form. Therefore, in this study to investigate the structure property relationship Co_3O_4 - Ti/$Na_2Ti_6O_{13}$ hybrid nanocomposites, the annealing process was done at 150 °C, 350 °C and 650 °C to understand their capacitive properties in different phases.

The visible apparent peak in the XRD patterns indicates the presence of both rutile and anatase phases of TiO_2, along with potential sodium hexa-titanates formation. The peaks seen at 13.7° and 28.5° were identified as corresponding to the (200) and (110) planes of sodium hexa-titanates [11]. The peaks observed at 31.9° were identified as belonging to the (110) plane of the rutile TiO_2 phase. This may occur due to the presence of Na ion, which is larger than the Ti ion, replacing it in the lattice and causing alterations in the structure. Through an annealing process, alterations can be changed in their phase and solidified. Research has indicated that Na addition can reduce the temperature of the anatase to rutile phase change, resulting in the creation of Ti/$Na_2Ti_6O_{13}$ nanocomposites containing mixed rutile/anatase phases of TiO_2. The high crystallinity of the nanocomposites structure is confirmed by the strong intensity of the nanowire's peaks. Similarly,

with Co_3O_4 the annealing temperature influence crystallize size and increases sharpness of peaks. The apparent peaks seen at 22.0° and 42.9° were identified as (111) and (311) cubic phases of Co_3O_4. The Scherrer equation yields an average crystalline size of 15.3 nm for Ti/$Na_2Ti_6O_{13}$ nanocomposites and 19.74 nm for Co_3O_4 - Ti/$Na_2Ti_6O_{13}$ hybrid nanocomposites, indicating a minor structural change due to the Co_3O_4 modification.

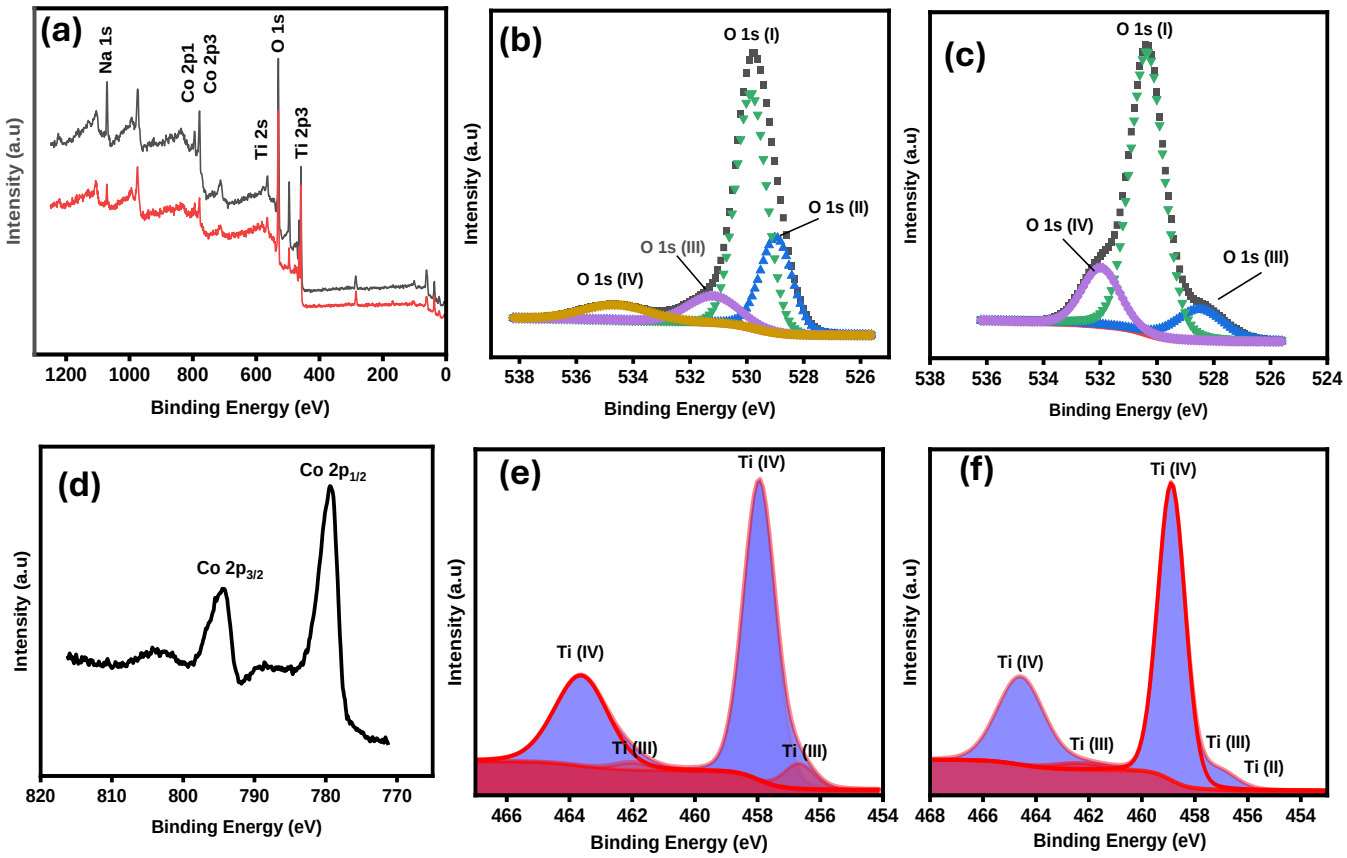

Figure 4-2: (a) XPS survey spectrum scans of Co_3O_4 - $Ti/Na_2Ti_6O_{13}$ after EC treatment, (b)(c) O 1s peaks of Co_3O_4 - $Ti/Na_2Ti_6O_{13}$ before and after EC treatment respectively, (d) Co 2p peaks Co_3O_4 - $Ti/Na_2Ti_6O_{13}$ after treatment (e) Ti 2p peaks of Co_3O_4 - $Ti/Na_2Ti_6O_{13}$ before and after EC treatment respectively.

XPS spectra were acquired for the titanium p1/2 and p3/2 orbitals as well as those for the O1s to investigate the surface chemical composition and how the EC treatment affected the formation of oxygen vacancies in the lattice structure of Co_3O_4 -$Ti/Na_2Ti_6O_{13}$. *Figure 4-2(a)* shows the survey spectrum, where the appearance of Na, Ti, O and Co signals are consistent with elemental composition of $Ti/Na_2Ti_6O_{13}$ and Co_3O_4 - $Ti/Na_2Ti_6O_{13}$ after their EC treatment. *Figure 4-2 (b)&(c)*, show the deconvoluted individual plots of O 1s pertaining to $Ti/Na_2Ti_6O_{13}$ and the modified Co_3O_4 - $Ti/Na_2Ti_6O_{13}$. Four major peaks at 528.97, 529.85, 531.18 and 534.68 eV attributed to oxides, hydroxides and oxygen vacancies were observed in both $Ti/Na_2Ti_6O_{13}$ and the

Co_3O_4 - Ti/$Na_2Ti_6O_{13}$ hybrid nanocomposites [10]. It reveals that the surface species do not change on modified electrodes due to the EC treatment process. *Figure 4-2(d)* shows XPS spectrum for Co 2p reveal two major peaks at binding energies of 780 and 795 eV which corresponds to Co $2p_{3/2}$ and Co $2p_{1/2}$ [12]. *Figure 4-2 (e)* reveals binding energies of Ti^{4+} and Ti^{3+} states were determined to be approximately 458.75 eV and 457.45 eV for Ti/$Na_2Ti_6O_{13}$ nanocomposites before EC treatment.

Figure 4-2(f) shows binding energies of Ti^{4+}, Ti^{3+}, and Ti^{2+} states that were determined to be approximately 457.94, 463.62, and 456.67 eV respectively. These binding energies correspond to Ti (IV)-O, Ti (III)-O and Ti (II)-O bonds in the TiO_2 rutile phase [13]. Following the EC treatment, it was evident of Ti (IV) decreased, while atomic percentage of Ti (III) and Ti (II) increased simultaneously. These results indicate an increase in defects within the Ti/$Na_2Ti_6O_{13}$ nanocomposites lattice after the EC treatment. It reveals that the surface species do not change on modified electrodes due to the EC treatment process. It was identified that upon the EC treatment of Ti/$Na_2Ti_6O_{13}$ nanocomposites showed an improved C_{sp} values. This trend was also true in case of Co_3O_4 - Ti/$Na_2Ti_6O_{13}$ hybrid nanocomposites. These trends of improved C_{sp} values via EC treatment and Co_3O_4 - Ti/$Na_2Ti_6O_{13}$ hybrid nanocomposites will be discussed in the later sections of this study.

4.3.2. Electrochemical Characterization of Co_3O_4 - $Na_2Ti_6O_{13}$

Electrochemical properties of Co_3O_4 - Ti/$Na_2Ti_6O_{13}$ hybrid nanocomposite electrodes were investigated using cyclic voltammetry (CV) at various scan rates in a 0.1 M H_2SO_4 electrolyte at room temperature. The CV curves were obtained and compared for hybrid nanocomposite electrodes annealed at 150°C, 350°C, and 650°C, as well as before and after electrochemical (EC) treatment. *Figure 4-3* CV curves of the Co_3O_4-Ti/$Na_2Ti_6O_{13}$ electrodes exhibited a partial rectangular shape, indicating electric double-layer capacitor (EDLC) behavior with redox peaks near 0.9 V, representing the pseudo capacitance behavior of cobalt. This demonstrates the synergistic effect of the Co_3O_4 - Ti/$Na_2Ti_6O_{13}$. The specific capacitance (Csp) values calculated from the CV curves showed a significant increase with increasing annealing temperature, from 120.69 F cm^{-2} g^{-1} at 150 °C, 248.68 F cm^{-2} g^{-1} at 350 °C 408.84 F cm^{-2} g^{-1} at 650 °C (at a scan rate of 10 mV/s). After EC treatment, the Csp values further increased to 142.51 F cm^{-2} $^{g-1}$, 301.41 F cm^{-2} g^{-1}, and 578.87 F cm^{-2} g^{-1} for the electrodes annealed at 150°C, 350°C, and 650 °C, respectively (at a scan rate of 10 mV/s). The increase in Csp after EC treatment is attributed to the introduction of oxygen vacancies. The plots of Csp versus scan rate showed a dramatic improvement in capacitance with increasing annealing temperature across all scan rates, with the most noticeable improvement observed for the electrodes annealed at 650°C. However, the specific capacitance decreased with increasing scan rate, due to faster redox reactions on the electrode [14].

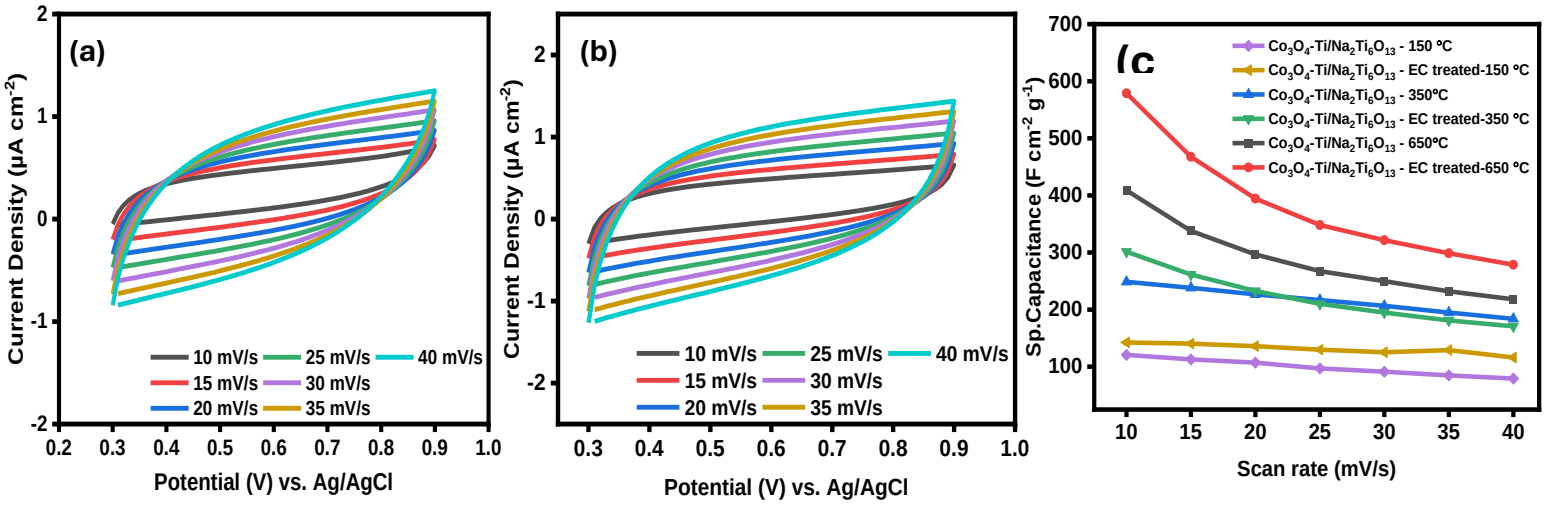

Figure 4-3: Cyclic voltammetry (CVs) curves for Co_3O_4 - $Ti/Na_2Ti_6O_{13}$ were obtained from a scan rate of 10 to 40 mV s^{-1} and annealed (a-b) Co_3O_4 - $Ti/Na_2Ti_6O_{13}$ annealed at 650°C before and after EC treatment step respectively. The specific capacitance of both (c) Co_3O_4 - $Ti/Na_2Ti_6O_{13}$ measured as a function of scan rate.

Galvanostatic charge and discharge (GCD) cycles, as shown in *Figure 4-4*, were conducted on Co_3O_4 - $Ti/Na_2Ti_6O_{13}$ hybrid nanocomposites in a 0.1 M H_2SO_4 electrolyte. The measurements were performed at current densities of 1, 2, 6, 8 and 10 µA within a potential window of 0-0.9 V vs. Ag/AgCl. The GCD curves exhibited suitable linear symmetric shapes across the tested current densities, indicating a significant contribution of fast and accessible double-layer capacitance (Cdl) to the overall capacitive behavior. GCD cycles were evaluated for each annealing temperature, exploring different charging and discharging rates. *Figures 4-4 (a) (b)* illustrate the GCD curves of Co_3O_4 - $Ti/Na_2Ti_6O_{13}$ at a current density of 1 µA for each annealing temperature. The discharge time increased consecutively from 150 to 650°C. The specific capacitance (Csp) values calculated from the GCD plots showed the highest Csp of 118.78 F cm^{-2} g^{-1} at a current density of 1 µA for the 650°C electrode, demonstrating the impact of temperature on electrochemical performance.

The electrodes were further subjected to electrochemical (EC) treatment to create oxygen vacancies and were tested again for GCD curves at 1 µA. The discharge time increased for each annealed temperature, indicating slower electrolyte ion transport [15]. The calculated Csp after EC treatment was 121.06 F cm^{-2} g^{-1} at 1 µA for the 650°C electrode. The results for the 650°C annealing temperature were focused on due to the longest charge-discharge time. It was observed that the charging/discharging time decreased at higher current densities due to the faster diffusion of ions on the electrode surface, affecting the charge storage capability [16]. This is illustrated in *Figures 4-4(c)(d)*, which show the GCD curves for the 650°C electrodes measured at various current densities of 1, 2, 6, 8, and 10 µA. The calculated Csp for Co_3O_4 - Ti/$Na_2Ti_6O_{13}$ before EC treatment was 118.78 F cm^{-2} g^{-1}, 70.45 F cm^{-2} g^{-1}, 45.75 F cm^{-2} g^{-1}, 25.43 F cm^{-2} g^{-1} and 9.64 F cm^{-2} g^{-1} at 1, 2, 6, 8 and 10 µA current densities, respectively. After EC treatment, the Csp was found to be 121.06 F cm^{-2} g^{-1} , 81.67 F cm^{-2} g^{-1}, 55.91 F cm^{-2} g^{-1} ,30.43 F cm^{-2} g^{-1} and 15.56 F cm^{-2} $g^{-1}$the same current densities.

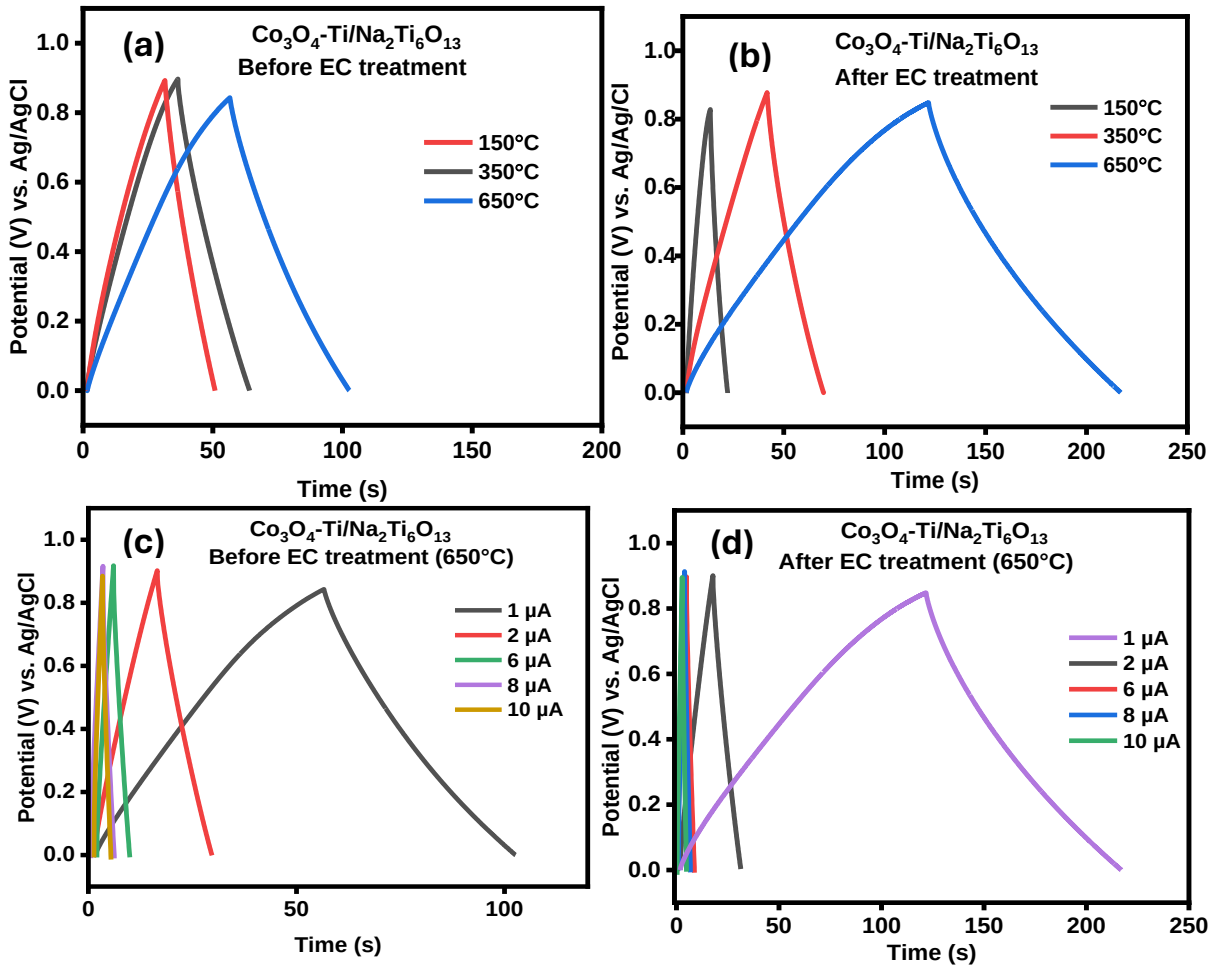

Figure 4-4: Galvanostatic charge-discharge curves (GCD) of (a) Co_3O_4 - $Ti/Na_2Ti_6O_{13}$ at different annealing temperatures before treatment, (b) after treatment, (c) GCD curves of 650°C collected at a current density of 1 µA, 2 µA, 6 µA, 8 µA and 10 µA before (d) and after EC treatment

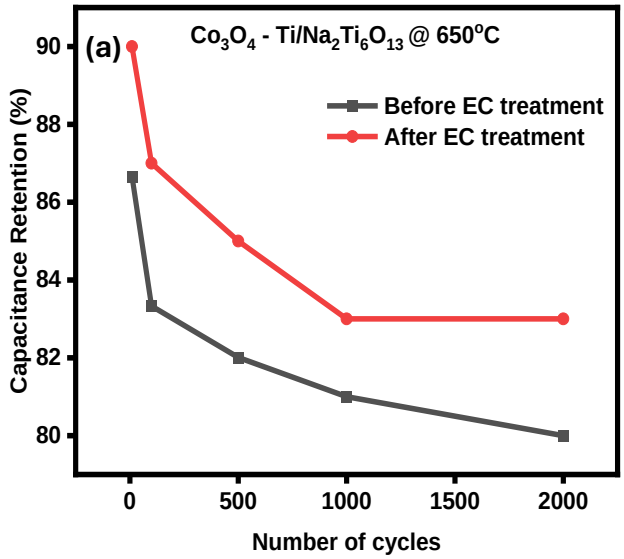

Figure 4-5: Cycling stability of Co_3O_4 - $Ti/Na_2Ti_6O_{13}$ at 650°C

The GCD analysis were obtained for 2000 cycles to get additional information on the cycling behaviour and stability of the electrode at 1 µA current density. *Figure 4-5* demonstrate the calculated capacitance retention of the electrodes annealed at 650 °C after 2000 cycles at about 80% and 83% at 1 µA for samples without and with EC treatment, respectively. Furthermore, the GCD curves of 650 °C remained unchanged, showing a symmetric and linear triangular shape after 2000 cycles and the stability of oxygen vacancies on lattice structure were demonstrated by the stability of electrodes after 2000 cycles.

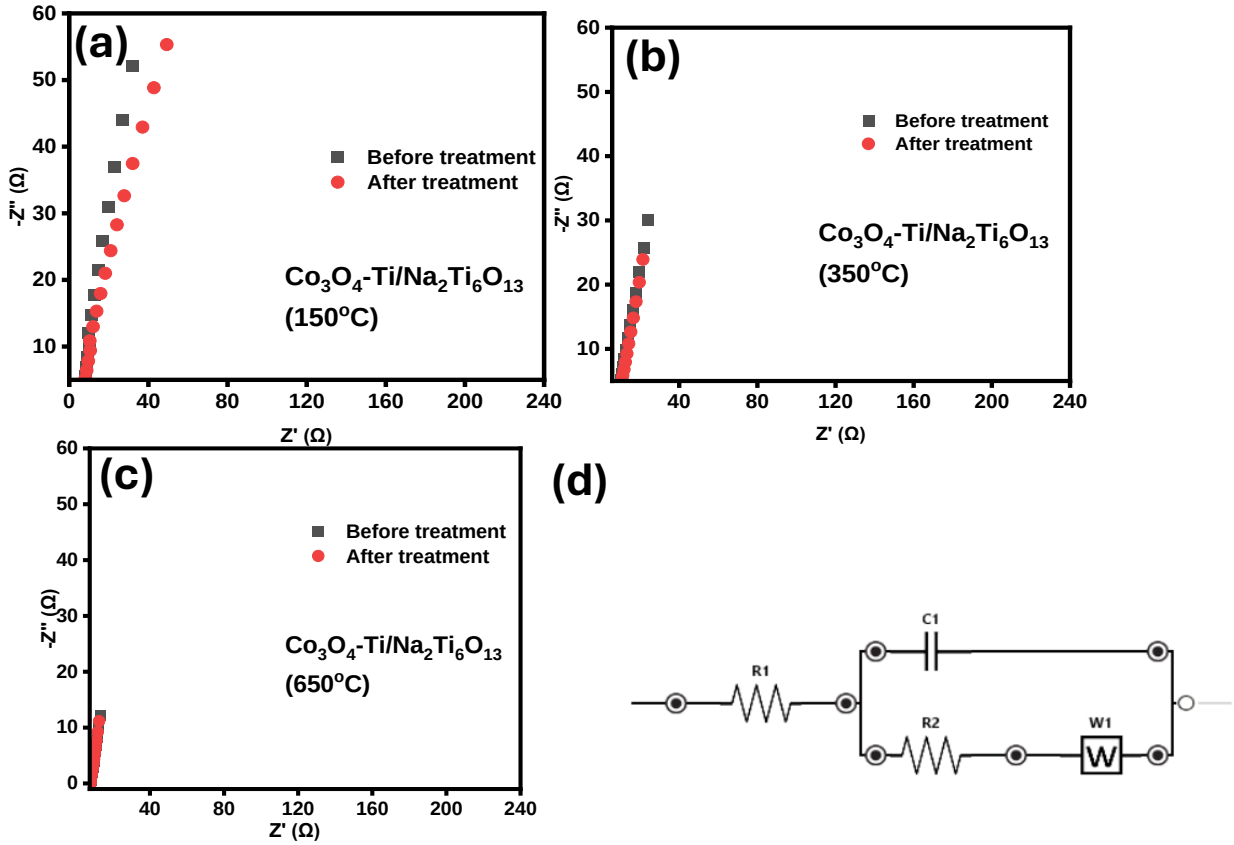

Figure 4-6: Nyquist plots of Co_3O_4 - $Ti/Na_2Ti_6O_{13}$ before and after treatment collected at frequencies from 100,000 Hz to 100 Hz; (a) 150 °C (b) 350 °C (c) 650 °C annealed temperature (d) equivalent circuit diagram

Electrochemical impedance tests were conducted on Co_3O_4 - $Ti/Na_2Ti_6O_{13}$ hybrid nanocomposite electrodes to assess their electrical conductivity and charge transfer resistance. *Figure 4-6* represent Nyquist plots of Co_3O_4 - $Ti/Na_2Ti_6O_{13}$ hybrid nanocomposite electrodes before and after electrochemical (EC) treatment at 150°C 350°C and 650°C. The tests were carried out in 0.1 M H_2SO_4 within a frequency range of 100,000 to 100 Hz and an electrode potential of 0.6 V.

To evaluate the charge transfer properties on the electrode surface, the Nyquist plots were fitted to an equivalent circuit model. This model includes R1 representing the electrolyte resistance, R2 representing the charge transfer at the electrode-electrolyte interface, C1 representing the capacitive behavior, and W1 representing the Warburg diffusion coefficient. The impedance intercept on the real axis at high frequencies corresponds to the equivalent series resistance (ESR)

of the system [17]. *Table 4-1* shows the calculated values of circuit diagram and the formation of semicircles on the Nyquist plots indicates the electrode resistance and material conductivity. The arc in the low-frequency region represents charge transfer reactions represent at *Figure 4-6 (b)*. The decrease in resistance values after EC treatment suggests the introduction of oxygen vacancies, leading to enhanced electrical conductivity. The 650°C electrodes exhibit a steeper slope in the low-frequency region, indicative of improved capacitive performance. EIS analysis comparing Co_3O_4 - Ti/$Na_2Ti_6O_{13}$ electrodes reveal a reduction in film resistance (R1) and charge transfer resistance (R2) with Co_3O_4 modification, accompanied by significantly higher capacitance. This indicates an improvement in the resistance and capacitance of the hybrid nanocomposite.

Table 4-1: Calculated values of an equivalent circuit diagram for samples before EC treatment and after EC treatment respectively

Samples	**Annealed Temperature (°C)**	**R1 (Ohms)**	**R2 (Ohms)**	**C1 (F)**	**W1**
Co_3O_4 modified sodium hexa-titanates	150	6.743	20.65	35.54	0.040
	350	3.541	12.53	46.35	0.256
	650	1.098	7.97	150.45	4.253
Samples	**Annealed Temperature (°C)**	**R1 (Ohms)**	**R2 (Ohms)**	**C1 (F)**	**W1**
Co_3O_4 modified sodium hexa-titanates	150	7.654	25.64	70.64	0.080
	350	5.705	10.53	100.34	0.146
	650	0.985	4.68	180.5	2.85

4.4. Conclusion

A facile process has been developed to grow $Na_2Ti_6O_{13}$ nanocomposites on a Ti metal substrate surface using a hydrothermal process. Subsequently, oxygen vacancies were successfully introduced into the lattice structure of the nanocomposites, which showed an observable enhancement in its specific capacitance (C_{sp}). The electrical conductivity and charge transfer significantly improved after introducing oxygen vacancies via EC treatment methodology. Cobalt oxide nanoparticles were synthesized through hydrothermal process and drop-casted on surface to create the hybrid-nanocomposite of the material and annealed at different temperatures for phase transformation. The Csp for Co_3O_4 - Ti/$Na_2Ti_6O_{13}$ was achieved to be 408.84 before EC treatment and 578.87 F cm^{-2} g^{-1} after EC treatment at a scan rate of 10 mV s^{-1}. The experiments demonstrate that the modified sodium hexa-titanates with Co_3O_4 nanoparticles can be used as an electrode material for high-performance supercapacitor applications in future.

4.5. References

[1] M. Armand and J.-M. Tarascon, "Building better batteries," *Nature*, vol. 451, no. 7179, pp. 652–657, Feb. 2008, doi: 10.1038/451652a.

[2] S. Mishra, P. Yogi, P. R. Sagdeo, and R. Kumar, "TiO2–Co3O4 Core–Shell Nanorods: Bifunctional Role in Better Energy Storage and Electrochromism," *ACS Appl. Energy Mater.*, vol. 1, no. 2, pp. 790–798, Feb. 2018, doi: 10.1021/acsaem.7b00254.

[3] S. Veeresh *et al.*, "Graphene oxide/cobalt oxide nanocomposite for high-performance electrode for supercapacitor application," *Journal of Energy Storage*, vol. 52, p. 104715, Aug. 2022, doi: 10.1016/j.est.2022.104715.

[4] P. Simon and Y. Gogotsi, "Materials for electrochemical capacitors," *Nature Mater*, vol. 7, no. 11, pp. 845–854, Nov. 2008, doi: 10.1038/nmat2297.

[5] G. Zhang and X. W. (David) Lou, "Controlled Growth of NiCo2O4 Nanorods and Ultrathin Nanosheets on Carbon Nanofibers for High-performance Supercapacitors," *Sci Rep*, vol. 3, no. 1, p. 1470, Mar. 2013, doi: 10.1038/srep01470.

[6] M. T. Greiner, L. Chai, M. G. Helander, W.-M. Tang, and Z.-H. Lu, "Transition Metal Oxide Work Functions: The Influence of Cation Oxidation State and Oxygen Vacancies," *Advanced Functional Materials*, vol. 22, no. 21, pp. 4557–4568, 2012, doi: 10.1002/adfm.201200615.

[7] J. Meyer *et al.*, "Metal Oxide Induced Charge Transfer Doping and Band Alignment of Graphene Electrodes for Efficient Organic Light Emitting Diodes," *Sci Rep*, vol. 4, no. 1, p. 5380, Jun. 2014, doi: 10.1038/srep05380.

[8] M. Amiri, J. Dondapati, J. Quintal, and A. Chen, "Sodium Hexa-Titanate Nanowires Modified with Cobalt Hydroxide Quantum Dots as an Efficient and Cost-Effective Electrocatalyst for Hydrogen Evolution in Alkaline Media," *ACS Appl. Mater. Interfaces*, vol. 14, no. 35, pp. 40021–40030, Sep. 2022, doi: 10.1021/acsami.2c11310.

[9] X. Zhao, Z. Cai, T. Wang, S. E. O'Reilly, W. Liu, and D. Zhao, "A new type of cobalt-deposited titanate nanotubes for enhanced photocatalytic degradation of phenanthrene," *Applied Catalysis B: Environmental*, vol. 187, pp. 134–143, Jun. 2016, doi: 10.1016/j.apcatb.2016.01.010.

[10] S. Arshadi Rastabi, R. Sarraf-Mamoory, G. Razaz, N. Blomquist, M. Hummelgård, and H. Olin, "Treatment of NiMoO4/nanographite nanocomposite electrodes using flexible graphite substrate for aqueous hybrid supercapacitors," *PLoS One*, vol. 16, no. 7, p. e0254023, 2021, doi: 10.1371/journal.pone.0254023.

[11] X. Chang, S. S. Thind, and A. Chen, "Electrocatalytic Enhancement of Salicylic Acid Oxidation at Electrochemically Reduced TiO2 Nanotubes," *ACS Catal.*, vol. 4, no. 8, pp. 2616–2622, Aug. 2014, doi: 10.1021/cs500487a.

[12] R. Kumar, A. Soam, and V. Sahajwalla, "Carbon coated cobalt oxide (CC-CO3O4) as electrode material for supercapacitor applications," *Mater. Adv.*, vol. 2, no. 9, pp. 2918–2923, May 2021, doi: 10.1039/D1MA00120E.

[13] S. Alkhalaf *et al.*, "Electrochemical energy storage performance of electrospun CoMn2O4 nanofibers," *Journal of Alloys and Compounds*, vol. 692, pp. 59–66, Jan. 2017, doi: 10.1016/j.jallcom.2016.09.005.

[14] Y. Zhang, X. Li, Z. Li, and F. Yang, "Evaluation of electrochemical performance of supercapacitors from equivalent circuits through cyclic voltammetry and galvanostatic

charge/discharge," *Journal of Energy Storage*, vol. 86, p. 111122, May 2024, doi: 10.1016/j.est.2024.111122.

[15] D. Ghosh, S. Giri, and C. K. Das, "Synthesis, characterization and electrochemical performance of graphene decorated with 1D NiMoO4·nH2O nanorods," *Nanoscale*, vol. 5, no. 21, pp. 10428–10437, Oct. 2013, doi: 10.1039/C3NR02444J.

[16] A. Sarkar, A. K. Singh, D. Sarkar, G. G. Khan, and K. Mandal, "Three-Dimensional Nanoarchitecture of BiFeO 3 Anchored TiO 2 Nanotube Arrays for Electrochemical Energy Storage and Solar Energy Conversion," *ACS Sustainable Chem. Eng.*, vol. 3, no. 9, pp. 2254–2263, Sep. 2015, doi: 10.1021/acssuschemeng.5b00519.

[17] X. Zheng *et al.*, "Understanding the structural and chemical evolution of layered potassium titanates for sodium ion batteries," *Energy Storage Materials*, vol. 25, pp. 502–509, Mar. 2020, doi: 10.1016/j.ensm.2019.09.032.

Chapter 5: Conclusion and Future Works

5.1 Conclusion

- An investigation of this research was conducted using two different metal oxides for the development of electrode materials for supercapacitor applications.
- Novel material, TiO_2-based sodium hexa- titanates was primarily used in LIBs applications and can be a potential candidate for supercapacitor applications
- Sodium Hexa-Titanates ($Na_2Ti_6O_{13}$) electrodes was successfully developed to grow on a Ti metal substrate surface using a hydrothermal process
- Additional fabrication of $Na_2Ti_6O_{13}$ with well-known Ruthenium oxide (RuO_2) that is known to have energy storage applications. The fabrication was successful, allowing for the fabrication of high-mass loading electrodes.
- The unique finding obtained from the work was the formation of long wires of titanates, where electrolyte ions can diffuse into the surface. This can lead to the development of new and effective materials
- Titanates were investigated with the new dopant cobalt oxide nanoparticles to see if the movement of electrolyte ions led to significant changes in how the electrolyte species diffuse the composite's porous structure, which yields different electrochemical performances.
- $Na_2Ti_6O_{13}$ had shown remarkable electrochemical performance through electrochemical measured specific capacitance, potentially leading to develop next-gen supercapacitors.

5.2. Future works

- This investigation has led to more potential work, different synthesis techniques can be explored for optimization of the structural features and controlled sized nanowires.
- Due to sodium hexa-titanates have great mechanical properties, integrating them into polymer composites or carbon-based materials can enhance their electrochemical performance and structural features.
- Optimization of material in different electrolyte systems such as organic and polymer with different concentration. This would assist in establishing whether nanocomposites are promising candidates for future applications.
- Furthermore, more characterization techniques such as TEM and FTIR would assist in further comparison with other nanocomposites.